SCOUR ANALYSIS OF THE INTERSTATE-35 AND CIMARRON RIVER CROSSING USING THE FESWMS-2DH AND SMS COMPUTER MODELS

By

MICHAEL T. BUECHTER

Bachelor of Science

University of Missouri at Rolla

Rolla, Missouri

1990

Submitted to the Faculty of the
Graduate College of the
Oklahoma State University
in partial fulfillment of
the requirements for
the Degree of
MASTER OF SCIENCE
May, 1997

SCOUR ANALYSIS OF THE INTERSTATE-35 AND

CIMARRON RIVER CROSSING USING THE

FESWMS-2DH AND SMS

COMPUTER MODELS

Thesis Approved:

Ali Tyapi

Thesis Advisor

Vernon G. Mast

Gerald D. Oberlander

Thomas C. Collins

Dean of the Graduate College

PREFACE

This study uses the commonly used scour prediction methods to analyze the October 1986 flood which damaged the bridges at the Interstate-35 and Cimarron River crossing. The hydraulic analysis of this site was completed using the FESWMS-2DH computer program. The FESWMS-2DH computer program considers the dynamics of flow in both directions and is well suited to analyze this complex site. The use of this computer program was greatly simplified by using the SMS computer program which allows data to be input and output in graphical environment. The results of this study demonstrate the validity of the commonly used scour equations and the usefulness of the FESWMS-2DH and SMS computer program.

I wish to express my sincere gratitude to the individuals who assisted me in this project and during my course work at Oklahoma State University. In particular I wish to thank my major advisor Dr. A. K. Tyagi for his guidance. I am also grateful to Dr. Mast and Dr. Oberlender, both for serving on my committee and their enlightening courses. I would also like to thank Ms. Ramona Wheately for constant support and encouragement.

Special thanks are due to Dr. Alan Zundel and the Engineering Computer Graphics Laboratory at Bingham Young University for both providing me with the SMS computer software and for their assistance in solving the flow problem. I would also like to thank Mr. Larry Arneson of the FHWA for his intelligent input and advice. Mr. Dale

Abernathie is also thanked for his valuable computer advice and his help in preparing the manuscript.

Additional thanks are due to the Oklahoma Department of Transportation Hydraulic Branch which provided the information needed for this study, along with an original version of the FESWMS-2DH computer program.

I would especially like to thank my wife, Mrs. Rita Buechter, for her constant support, encouragement and for typesetting the manuscript.

TABLE OF CONTENTS

LIST OF TABLES

LIST OF FIGURES

FIGURE PAGE

NOMENCLATURE

A_e = an element surface

D_{50} = median diameter of the bed material in feet

FESWMS-2DH = Finite Element Surface Water Modeling System: Two-Dimensional Flow in a Horizontal Plane

f = a known function

g = acceleration due to gravity

H = water depth

L = a differential operator

N_i = the assumed interpolation function

n = Manning's n

n_x & n_y = the direction cosines between outward normal to the boundary and the positive x and y directions, respectively

O.D.O.T. = Oklahoma Department of Transportation

O.F. = overflow

Q_i = total source / sink flow attributed to node I

Q_5 = runoff produced at a 5 year event

Q_{10} = runoff produced at a 10 year event

Q_{25} = runoff produced at a 25 year event

Q_{50} = runoff produced at a 50 year event

Q_{52} = runoff produced at 52 year event

Q_{100} = runoff produced at a 100 year event

Q_{500} = runoff produced at a 500 year event

SCS = Soil Conservation Service

SMS = surface water modeling system

s_e = an element boundary

subscript_o = the known values at the start of a time step

Δt = the length of the time step

U = horizontal velocity in the x direction at a point along the vertical coordinate

USGS = United States Geological Survey

u = the unknown nodal variable

V = horizontal velocity in the y direction at a point along the vertical coordinate

V_c = the critical velocity above which bed material of a size D_{50} and smaller will be transported

W_1 = bottom width of upstream main channel

W_2 = bottom width of main channel in contracted section

y = flow depth

y_1 = average depth in upstream channel

y_2 = average depth in contracted section

z = the vertical direction

z_b = the bed elevation

z_s = the water surface elevation

$\alpha_x = \arctan (\partial z_b / \partial x)$

$\alpha_y = \arctan (\partial z_b / \partial y)$

$\alpha_z = \arccos (1 - \cos^2\alpha_x - \cos^2\alpha_y)$

β_{uu}, β_{vv} & β_{vv} = momentum flux correction coefficients that account for the variation of velocity in the vertical direction

θ = a weighting coefficient ranging from 0.5 to 1

ρ = water mass density

τ_{bx} & τ_{by} = bed shear stress acting in the x and y directions, respectively

τ_{sx} & τ_{sy} = surface shear stress acting in the x and y directions, respectively

τ_{xx}, τ_{xy} & τ_{yy} = shear stress caused by turbulence where, for example, τ_{xy} is the shear stress acting in the x direction on a plane that is perpendicular to the y direction

τ_2 = average bed shear stress in the contracted section

Ω = Coriolis parameter

CHAPTER 1

INTRODUCTION

Statement of the Problem

Crossing History

Interstate-35 crosses the Cimarron River at the border of Payne and Logan Counties, north of Guthrie, Oklahoma. Prior to 1988 the four lanes of Interstate-35, two lanes in each direction separated by a 40 foot median and shoulders, crossed the Cimarron River and its floodplain at this location on two main bridges and a series of eight overflow bridges. However, these bridges were severely damaged by a large flood in October of 1986. As a result of this damage the previously existing bridges were replaced by the existing structures in 1988. The existing structures include two main bridges over the Cimarron River and two large overflow bridges on the floodplain.

As mentioned previously, prior to 1988 Interstate-35 crossed the Cimarron River on two main bridges and eight overflow bridges. The two main bridges were located in a parallel installation on the southern edge of the river valley, over the river channel. The eight overflow bridges were located on the floodplain in series of four parallel installations. The overflow structures were placed at increments of 900 feet, 450 feet, 650 feet apart. The main bridges were 805 feet long while the overflow bridges ranged in length from 160 to 280 feet. The main bridges had a flowline of approximately 870.2 feet while the flowlines of the overflow bridges ranged from 885 feet to 887 feet.

The existing main structures are also located on the southern edge of the river

valley over the main channel. The two overflow structures are located in a parallel installation on the northern edge of the river valley. The main bridges are 800 feet long and have a flowline elevation of 870.5 feet. The overflow bridges are 1,360 feet long and have a flowline elevation of 887.0 feet.

Flood Events

The October 1986 flood is one of the two most severe floods on record for this site. The October 1986 flood had a recorded high water surface elevation of 898.0 feet and a recorded peak flow of 156,000 cubic feet per second, approximately a Q_{52} event. The other of the two most severe floods which occurred at this site, occurred in May of 1957. No discharge information is available for this event, however, a high water surface elevation of 899.0 feet was recorded.

Description of Watershed

As mentioned previously, Interstate-35 crosses the Cimarron River at the border of Payne and Logan Counties in the state of Oklahoma. Before entering Oklahoma, the Cimarron River originates in New Mexico. The river first enters and exits the state of Oklahoma at Cimarron County. Secondly, the river reenters the state at Beaver County and exits at Harper County. Finally, the river enters the state for a third and final time where it forms part of the eastern portion of the Harper County line. Then the river flows in a southeasterly direction to its termination at the Keystone Reservoir. Approximately 17,505 square miles of watershed contribute runoff to the river up to the crossing with Interstate-35. Of these 17,505 square miles, approximately 4,296 square miles are

controlled by SCS water detention structures.

Generally, the river valley varies in width from 0.8 to 1.2 miles. The river valley is approximately one mile in width with high banks at the Interstate-35 crossing. The main channel is 700 to 2,000 feet wide and, like many mature rivers, it is highly meandering. Currently the river is located at the southern edge of the floodplain and makes a sharp turn towards the east to go under the main structure. This condition existed at the time of the October 1986 flood and may have contributed to the large amount of scour which occurred during this flood. History indicates that the meander just upstream of the Interstate-35 crossings is moving downstream causing the main channel to move to the north of the floodplain.

Scope of the Investigation

The scope of this investigation is to apply advanced hydraulic and scour analysis to the October 1986 flood and previously existing structures at the Interstate-35 and Cimarron River crossing. From this analysis, scour depths can be calculated at the overflow bridges. The commonly used scour equations are based on theoretical assumptions, and studies of sand bed flumes, and correlated with little field collected data. Therefore, the results of this study will allow comparison of collected data to calculated scour values. This comparison should help validate the use of the scour equations as a design tool.

CHAPTER II

FINITE ELEMENT ANALYSIS

General

The finite element method is a numerical procedure which can produce approximate solutions to the initial boundary value partial differential equations common to physics and engineering. This method was originally conceived by engineers to analyze aircraft structural systems. However, the rapid development of the high speed digital computer led to the continuous development and application of finite element techniques to a wide range of engineering problems, including surface water flow problems. Lee and Froehlich (1986) published a detailed review of the literature discussing the application of finite element solutions to the equations of two dimensional surface water flow in a horizontal plane. Additionally, Finnie and Jeppson (1991) presented a method for solving turbulent flows with finite elements.

Solution Technique

The FESWMS-2DH computer program uses the Galerkin finite element method to solve the governing system of differential equations which describe surface water flow. Any finite element analysis solution begins by dividing the area of interest into a number of elements. These elements are usually triangular or quadrangular in shape and can be easily arranged to fit complex boundaries. Elements are defined at a number of points situated on the boundary and interior of the elements. These points are referred to as nodes. Values of the dependent variables are then approximated at these node points

using a set of interpolation or shape functions. In the FESWMS-2DH computer program, mixed interpolation is used to help stabilize the solution. Quadratic interpolation functions are used to interpolate depth averaged velocities and linear functions are used to interpolate flow depth.

To form a set of equations for each element the method of weighted residuals is applied to the governing differential equations. Various approximations of the dependant variables are then substituted into the governing equations which generally are not satisfied exactly, resulting in residuals. These residuals are made to vanish, in an average sense, when they are multiplied by a weighting function and summed at every point in the solution domain. In Galerkin's method the weighting functions are the same as the interpolation functions. By requiring the summation of the weighted residuals to equal zero, the finite element equations take on an integral form. Coefficients of the equations are integrated numerically and all the element equations are assembled to obtain a global system of equations which are solved simultaneously. Because this system of equations is nonlinear, Newton's iterative method as outlined by Zienkiewicz (1977) is used to solve them.

Basic Concepts

The fundamental concept of the finite element method is to divide the problem domain into a finite number of small regions called finite elements. Many convenient shapes are available for this purpose including triangles and quadrilaterals. Within each of these elements it is assumed that the value of a continuous quantity can be approximated by a set of piecewise-smooth functions using the values of that quantity at a

finite number of points. The piecewise-smooth functions are known as interpolation or shape functions. The points at which the continuous quantity is defined are called node points. The behavior of the solution throughout the assemblage of elements is described by the interpolation functions, once the unknown nodal quantities are found.

Once the elements and their interpolation functions have been chosen the derivation of the element equations may be achieved by several methods. These methods include direct methods, variational methods, or weighted residual methods. Although these methods provide a means of forming the element equations they are not directly related to the finite element method.

Weighted residual methods are general techniques for obtaining approximate solutions to linear and non-linear partial differential equations and include collation, least squares, and Galerkin methods. In all these, the unknown solution is approximated by a set of interpolation functions containing adjustable constants or functions. The chosen constants define the type of weighted residual method and attempt the "best" approximation of the exact solution.

As mentioned previously the particular weighted residual methods differ from one another in the choice of the weighting functions. In the method most used to derive finite-element equations, known as Galerkin's method, the weighting functions are chosen to be the same as the interpolation functions of the trial solution. Therefore, in Galerkin's method, $W_i = N_i$ for I = 1, 2, ..., m. Thus Galerkin's method requires that:

$$\int_R N_i \, (L \, \hat{u} - f) \, d \, R = 0 \qquad \text{I} = 1, 2, ..., \text{m} \qquad (2\text{-}1)$$

where

N_i = the assumed interpolation function

L = a differential operation

u = the unknown nodal variable

f = a known function

R = the domain

Additionally, the differential equation of a problem can be written as:

$$L\ u\ -\ f\ =\ 0 \tag{2-2}$$

The left hand side of Equation 2-1 can be written as the sum of expressions governing the behavior of Equation 2-2 on individual elements. The variable u can be approximated with respect to an element as:

$$\hat{u}^{(e)} = \sum_{i=1}^{n} N_i^{(e)} u_i^{(e)} \tag{2-3}$$

Where the superscript (e) denotes the restriction of the relevant variable or function to an element. Then the left hand side of Equation 2-1 can be written as the sum of expressions of the form:

$$\int_{R^{(e)}} N_i^{(e)}\ (L\hat{u}^{(e)}\ -\ f^{(e)})\ dR^{(e)} \qquad \text{I} = 1, 2, ..., \text{n} \tag{2-4}$$

where,

$R^{(e)}$ = the element domain

$f^{(e)}$ = the defined element function

A set of expressions like Equation 2-4 is written for each element in the network.

The assembly of element expressions results in a set of global algebraic equations, which must be solved simultaneously. In a finite element solution, the values of a quantity at the node points are the unknowns. The behavior of the solution within the entire assemblage of elements is described by the element interpolation functions and the node point values, after they have been found.

The basic idea of the finite element method is that a solution domain of arbitrary shape can be discretized by assumptions of elements in such a way that a sequence of approximate solutions defined on successively more defined discretizations will converge to the exact solution of the governing differential equations. The shapes of the elements chosen to model a region, along with the order of approximation desired, will determine the interpolation functions, N_i, which are used. Additionally, the interpolation functions need to satisfy certain criteria so that convergence of the numerical solution to an exact solution of the governing differential equations can be achieved. Because of these reasons most finite element networks consist of elements that are geometrically fairly simple. Common two dimensional elements are shown in Figure 1, Examples of Two Dimensional Elements. Although it is conceivable that many types of functions could be used as interpolation functions, almost all finite element solutions use polynomials because of their relative simplicity.

Governing Equations

In many surface water flow problems of practical engineering concern, the width to depth ratio of the water body is very large. In these instances the three dimensional

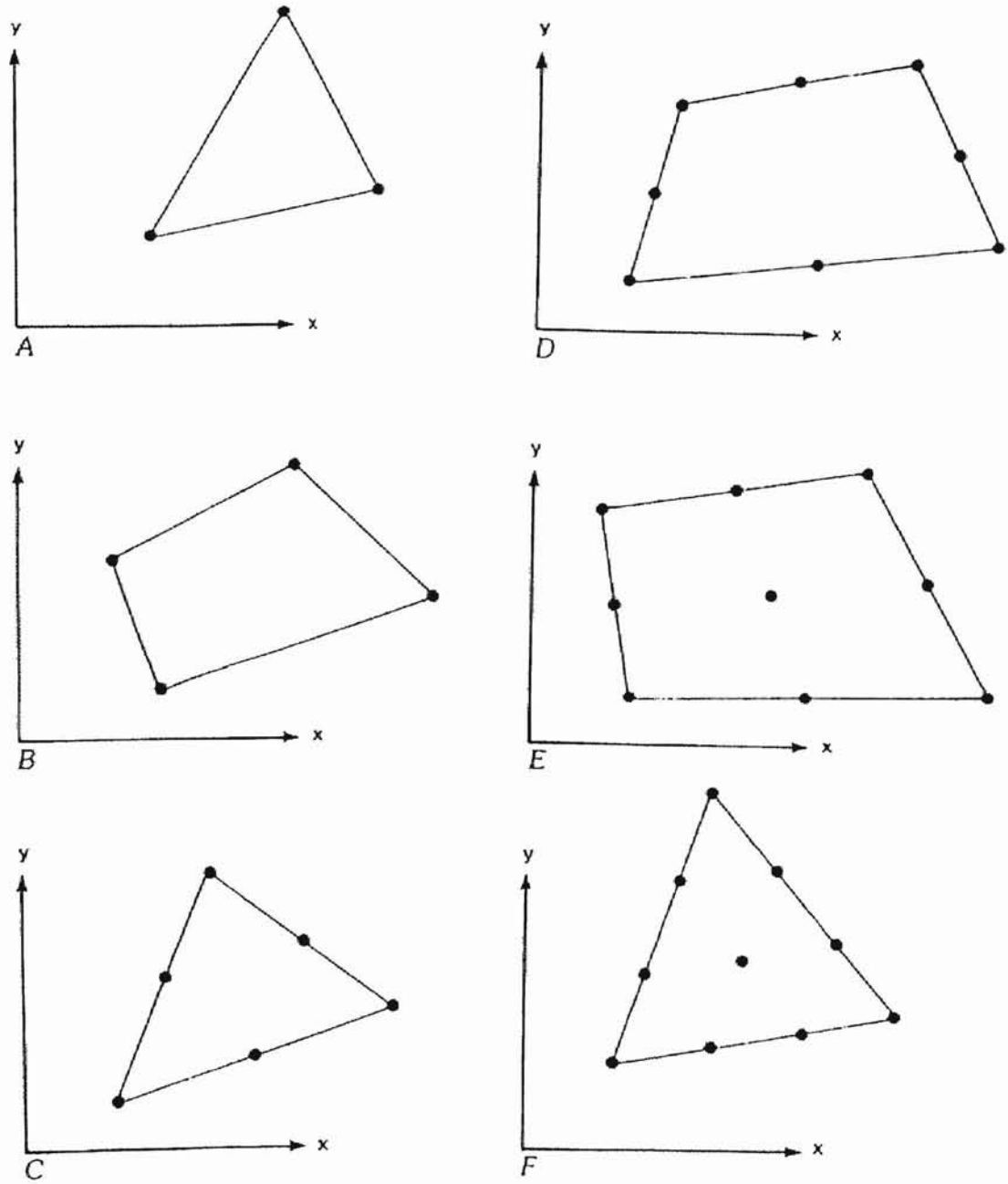

Figure 1. Examples of Two Dimensional Elements: (A) Three-node triangle; (B) Four-node quadrilateral; (C) Six-node triangle; (D) Eight-node quadrilateral; (E) Nine-node quadrilateral; (F) Ten-node triangle [Source: Lee and Froehlich, 1986, p.8]

nature of the flow may be ignored and a two dimensional flow application may be used. Cases in which flows may be mostly two dimensional in character include shallow coastal areas, harbors, estuaries, rivers and floodplains.

The FESWMS-2DH computer program calculates depth averaged horizontal velocities, flow depths, and the time derivatives of these quantities if a time dependant flow is modeled. As with any numerical model, a fundamental requirement of the FESWMS-2DH program is that a satisfactory quantitative description of the physical processes that are involved must be made. The equations that govern depth averaged surface water flow account for the effects of friction, wind induced stresses at the water surface, fluid stresses caused by turbulence, and the effect of the earth's rotation.

Steady State Solution

The equations that govern hydrodynamic behavior of a Newtonian fluid are based on the concepts of conservation of mass (continuity) and momentum (motion). As mentioned previously, for many practical surface water flow applications, knowledge of the full three dimensional flow structure is not required, and it is sufficient to use mean flow quantities in two perpendicular horizontal directions. By integrating the three dimensional equations over the water depth and assuming a constant fluid density, a set of three equations appropriate for modeling flow in shallow water bodies is obtained.

The coordinate system and variables used to obtain these equations are illustrated in Figure 2, Diagram of Coordinates System Axes. Depth-averaged velocity is illustrated in Figure 3, Illustration of Depth Averaged Velocities. Because the flow is assumed to be in a horizontal direction, it is convenient to use a right hand Cartesian coordinate system

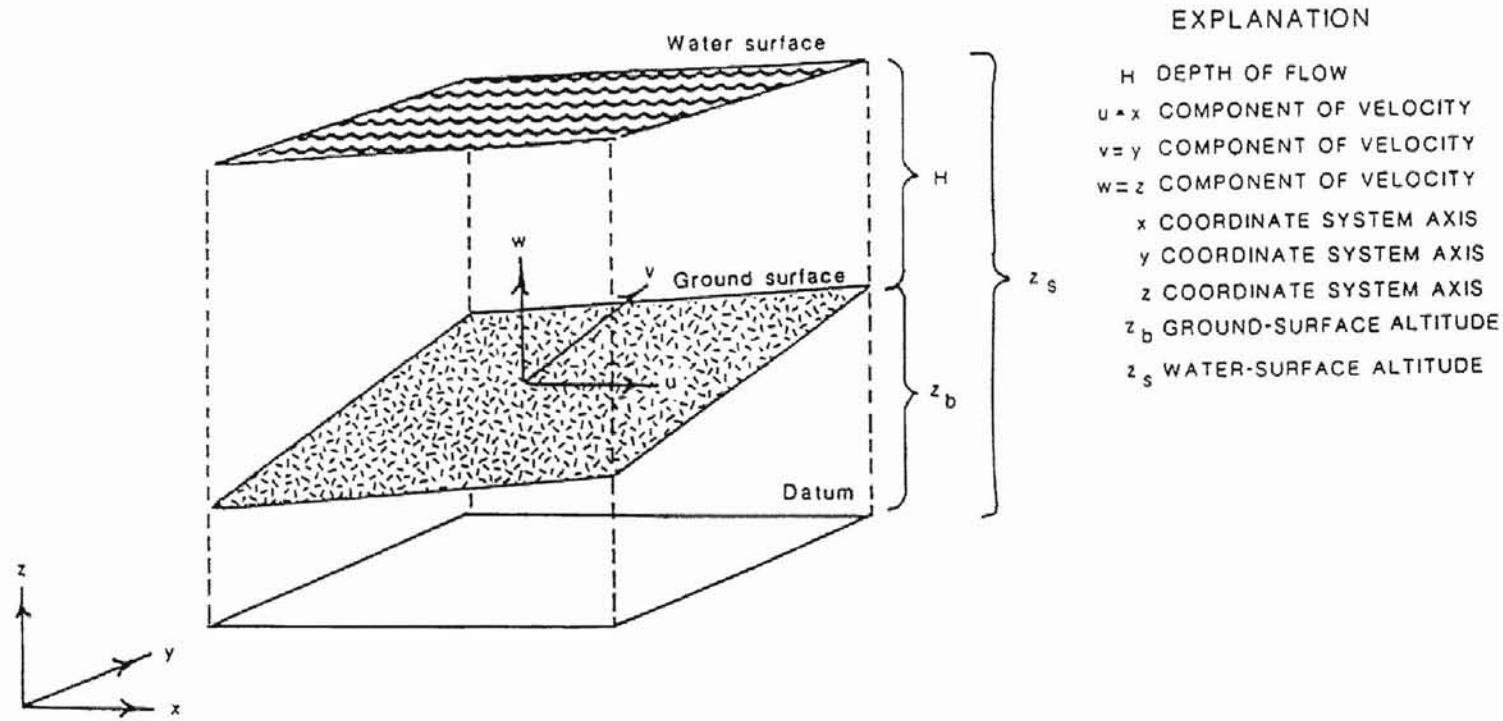

Figure 2. Diagram of Coordinate System Axes [Source: Gilbert and Myers, 1989, p.6]

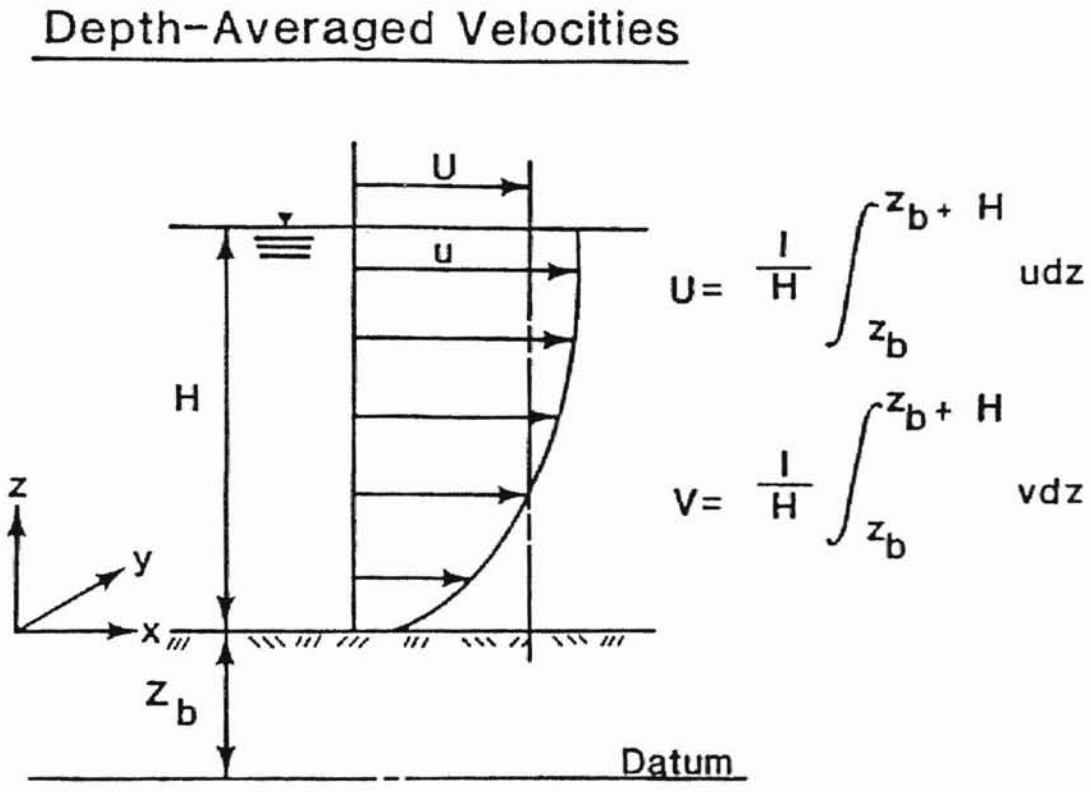

Figure 3. Illustration of Depth Averaged Velocity [Source: Froehlich, 1992, p. 4.3]

with the x and y axes in the horizontal planes and the z axis directed upward. The depth averaged velocity components in the horizontal x and y coordinate directions, respectively, are defined as follows:

$$U = \frac{1}{H} \int_{z_b}^{z_s} u \, dz \tag{2-5}$$

$$V = \frac{1}{H} \int_{z_b}^{z_s} v \, dz \tag{2-6}$$

where

H = the water depth

z_s = the vertical direction

z_b = the bed elevation

U = horizontal velocity in the x direction at a point along the vertical coordinate

V = horizontal velocity in the y direction at a point along the vertical coordinate

and

$z_s = z_b + H$ = the water surface elevation

Chaudhry (1993) presents a through derivation of the depth averaged surface water flow equations completed by integrating the three dimensional mass and momentum transport equations with respect to the vertical coordinate from the bed to the water surface and assuming that vertical velocities and accelerations are negligible. The

vertically integrated momentum equations are written as:

$$\frac{\partial(HU)}{\partial t} + \frac{\partial}{\partial x}\left(\beta_{uu}HUU + (\cos\alpha_x\cos\alpha_z)^2\,\frac{1}{2}gH^2\right) + \frac{\partial}{\partial y}(\beta_{uv}HUV) + \cos\alpha_x gH\frac{\partial z_b}{\partial x} - \Omega HV + \frac{1}{\rho}\left[\tau_{bx} - \tau_{sx} - \frac{\partial(H\tau_{xx})}{\partial x} - \frac{\partial(H\tau_{xy})}{\partial y}\right] = 0 \quad (2\text{-}7)$$

for flow in the x direction, and

$$\frac{\partial(HV)}{\partial t} + \frac{\partial}{\partial x}(\beta_{uv}HVU) + \frac{\partial}{\partial y}\left(\beta_{vv}HVV + (\cos\alpha_y\cos\alpha_z)^2\,\frac{1}{2}gH^2\right) + \cos\alpha_y gH\frac{\partial z_b}{\partial y} + \Omega HU + \frac{1}{\rho}\left[\tau_{by} - \tau_{sy} - \frac{\partial(H\tau_{yx})}{\partial x} - \frac{\partial(H\tau_{yy})}{\partial y}\right] = 0 \quad (2\text{-}8)$$

for flow in the y direction, where

β_{uu}, β_{uv}, and β_{vv} = momentum flux correction coefficients that account for the variation of velocity in the vertical direction

$\propto_x = \arctan(\partial z_b / \partial x)$

$\propto_y = \arctan(\partial z_b / \partial y)$

$\propto_z = \arccos(1 - \cos^2\propto_x - \cos^2\propto_y)$

g = gravitational acceleration

Ω = Coriolis parameter

ρ = water mass density, which is considered constant

τ_{bx} and τ_{by} = bed shear stress acting in the x and y directions, respectively

τ_{sx} and τ_{sy} = surface shear stress acting in the x and y directions, respectively

τ_{xx}, τ_{xy}, and τ_{yy} = shear stresses caused by turbulence where, for example, τ_{xy} is the shear stress acting in the x direction on a plane that is perpendicular to the y direction

The vertically integrated mass transport, continuity equation is:

$$\frac{\partial H}{\partial t} + \frac{\partial (HU)}{\partial x} + \frac{\partial (HV)}{\partial y} = q \qquad (2\text{-}9)$$

The bottom friction coefficient, used to compute the bed shear stress, may be computed as:

$$c_f = g / C^2 \qquad (2\text{-}10)$$

where

C = the Chezy discharge coefficient

or as

$$c_f = g\, n^2 / 2.208\, H^{1/3} \qquad (2\text{-}11)$$

where

n = the Manning's roughness coefficient

The effect of turbulence is modeled using Boussinesq's eddy viscosity concept. Boussinesq's eddy viscosity concept assumes that the turbulent stresses are proportional to the depth averaged velocity gradients. The eddy viscosity is defined so that when it is multiplied by the mean velocity gradients, the appropriate depth averaged stresses due to turbulence are obtained. Therefore, the eddy viscosity is not a true depth averaged quantity in the mathematical sense.

Finite element formulations for the residuals of the depth averaged flow equations, where the summation is with respect to all elements, written at node I are:

$$f_{U_i} \equiv \sum_e \int_{A_e} \left\{ N_i \left[H\frac{\partial U}{\partial t} + U\frac{\partial H}{\partial t} + gH\frac{\partial z_b}{\partial x} - \Omega HV + \frac{1}{\rho}(\tau_{bx} - \tau_{sx}) \right] + \right.$$
$$\left. \frac{\partial N_i}{\partial x}\left[-\beta HUU - \frac{1}{2}gH^2 + 2\tilde{\nu}H\frac{\partial U}{\partial x} \right] + \frac{\partial N_i}{\partial y}\left[-\beta HUV + \tilde{\nu}H\left(\frac{\partial U}{\partial y} + \frac{\partial U}{\partial y} \right) \right] \right\} dA_e + \quad (2\text{-}12)$$
$$\sum_e \int_{A_e} N_i \left\{ \left[\left(\beta HUU + \frac{1}{2}gH^2 \right)\eta_x + \beta HUV\eta_y \right] - \left[2\tilde{\nu}H\frac{\partial U}{\partial x}\eta_x + \tilde{\nu}H\left(\frac{\partial U}{\partial y} + \frac{\partial V}{\partial x} \right)\eta_y \right] \right\} dS_e$$

for flow in the x-direction, and

$$f_{V_i} \equiv \sum_e \int_{A_e} \left\{ N_i \left[H\frac{\partial V}{\partial t} + V\frac{\partial H}{\partial t} + gH\frac{\partial z_b}{\partial y} + \Omega HU + \frac{1}{\rho}(\tau_{by} - \tau_{sy}) \right] + \right.$$
$$\left. \frac{\partial N_i}{\partial x}\left[-\beta HUV + \tilde{\nu}H\left(\frac{\partial U}{\partial y} + \frac{\partial V}{\partial x} \right) \right] + \frac{\partial N_i}{\partial y}\left[-\beta HVV - \frac{1}{2}gH^2 + 2\tilde{\nu}H\frac{\partial V}{\partial y} \right] \right\} dA_e + \quad (2\text{-}13)$$
$$\sum_e \int_{A_e} N_i \left\{ \left[\beta HUV\eta_x + \left(\beta HVV + \frac{1}{2}gH^2 \right)\eta_y \right] - \left[\tilde{\nu}H\left(\frac{\partial U}{\partial y} + \frac{\partial V}{\partial x} \right)\eta_x + 2\tilde{\nu}H\frac{\partial V}{\partial y}\eta_y \right] \right\} dS_e$$

for flow in the y direction, where

A_e = an element surface

s_e = an element boundary

n_x and n_y = the direction cosines between the outward normal to the boundary and the positive x and y directions, respectively

All second order derivatives in the moment expressions have been integrated by parts using the Green-Gauss theorem. Reduction of the order of the expressions in this way allows use of quadratic functions to interpolate velocities. Integration by parts of the direction terms simplifies the finite element equation formulation. Integration by parts of

the pressure terms facilitates application of normal stress boundary conditions. The last boundary integral in square brackets ([ ]) in the two momentum residual expressions represents the lateral shear stresses resulting from the transport of momentum by turbulence.

The expression for the weighted residual of the continuity equation is:

$$f_{H_i} \equiv \sum_e \int_{A_e} M_i \left[\frac{\partial H}{\partial t} + H\frac{\partial U}{\partial x} + U\frac{\partial H}{\partial x} + H\frac{\partial V}{\partial y} + V\frac{\partial H}{\partial y} \right] dA_e - Q_i \qquad (2\text{-}14)$$

where

$$Q_i = \sum_e \int_{A_e} M_i \; q \; dA_e \qquad (2\text{-}15)$$

is the total source/sink flow attributed to node I

Time Derivatives

The residuals expressions 2-12, 2-13, and 2-14, given above, apply to a particular instant in time. For a steady state solution all the time derivatives are equal to zero and do not need to be evaluated. However, if the solution is time dependent, the residuals need to be integrated with respect to both time and space. Time integration is accomplished by using an implicit finite difference representation of the time derivatives. For example, the derivative of U with respect to time at the end of a time step is:

$$\frac{\partial U}{\partial t} = \frac{1}{\theta \Delta t} (U - U_o) - \frac{(1 - \theta)}{\theta} \left(\frac{\partial U}{\partial t}\right)_0 \qquad (2\text{-}16)$$

where

θ = a weighting coefficient ranging from 0.5 to 1

Δt = the length of the time step

subscript $_o$ = the known values at the start of a time step

For $\theta = 0$, the time integration scheme is explicit (forward Euler), for $\theta = 1$, the time integration scheme is implicit (backward Euler), and for $\theta = 0.5$, a trapezoidal (Crank-Nicholson) time integration scheme results. Setting θ equal to 0.67 can provide an accurate and stable solution for even relatively large time steps. The expressions for $\partial U / \partial t$ can be rearranged as:

$$\frac{\partial U}{\partial t} = \alpha U - \beta_1 \tag{2-17}$$

where

$$\alpha = \frac{1}{\theta \Delta t} \tag{2-18}$$

and

$$\beta_1 = \alpha U_o + \frac{(1 - \theta)}{\theta} \left(\frac{\partial U}{\partial t}\right)_o \tag{2-19}$$

where

β_1 = only quantities that are known at the start of a time step

In a similar manner, time derivatives of V and M are defined as:

$$\frac{\partial V}{\partial t} = \alpha V - \beta_2 \tag{2-20}$$

and

$$\frac{\partial H}{\partial t} = \alpha H - \beta_3 \tag{2-21}$$

where

$$\beta_2 = \alpha V_o + \frac{(1 - \theta)}{\theta} \left(\frac{\partial V}{\partial t}\right)_o \tag{2-22}$$

Using the procedure just outlined the expressions for derivatives of residuals are written for node I with respect to variables at node j. The derivative expressions for the residual of the conservation of momentum equation in the x direction are:

$$\begin{aligned}\frac{\partial f_{U_i}}{\partial U_j} \equiv & \sum_e \int_{A_e} \left\{ N_i N_j \left[\alpha H + \frac{\partial H}{\partial t} + \frac{\tau_{bx}}{\rho} \frac{2U^2 + V^2}{U(U^2 + V^2)} \right] \right. \\ & \left. + \frac{\partial N_i}{\partial x} N_j [-2\beta HU] + \frac{\partial N_i}{\partial x} \frac{\partial N_j}{\partial x} [2\tilde{\nu} H] + \frac{\partial N_i}{\partial y} N_j [-\beta HV] + \frac{\partial N_i}{\partial y} \frac{\partial N_j}{\partial y} [\tilde{\nu} H] \right\} dA_e \\ & + \sum_e \int_{S_e} \left\{ N_i N_j \left[2\beta HU\eta_x + \beta HV\eta_y \right] - N_i \frac{\partial N_j}{\partial x} \left[2\tilde{\nu} H\eta_x \right] - N_i \frac{\partial N_j}{\partial y} \left[\tilde{\nu} H\eta_x \right] \right\} dS_e \end{aligned} \tag{2-23}$$

$$\begin{aligned}\frac{\partial f_{U_i}}{\partial U_j} \equiv & \sum_e \int_{A_e} \left\{ N_i N_j \left[-\Omega H + \frac{\tau_{bx}}{\rho} \frac{V}{U^2 + V^2} \right] + \frac{\partial N_i}{\partial y} N_j [-\beta HU] + \frac{\partial N_i}{\partial y} \frac{\partial N_j}{\partial x} [\tilde{\nu} H][\tilde{\nu} H] \right\} dA_e \\ & + \sum_e \int_{S_e} \left\{ N_i N_j [\beta HU\eta_y] - N_i \frac{\partial N_j}{\partial x} [\tilde{\nu} H\eta_y] \right\} dS_e \end{aligned} \tag{2-24}$$

and

$$\frac{\partial f_{U_i}}{\partial H_j} \equiv \sum_e \int_{A_e} \left\{ N_i M_j \left[\alpha U + \frac{\partial U}{\partial t} - \Omega V + g\frac{\partial z_b}{\partial x} + \frac{\tau_{bx}}{\rho c_f}\frac{\partial c_f}{\partial H} \right] \right.$$
$$\left. + \frac{\partial N_i}{\partial x} M_j \left[-\beta UU - gH + 2\tilde{\nu}\frac{\partial U}{\partial x} \right] + \frac{\partial N_i}{\partial y} M_j \left[-\beta UV + \tilde{\nu}\left(\frac{\partial U}{\partial y} + \frac{\partial V}{\partial x} \right) \right] \right\} dA_e \qquad (2\text{-}25)$$
$$+ \sum_e \int_{S_e} \left\{ N_i M_j \left[\beta UU + gH + 2\tilde{\nu}\frac{\partial U}{\partial x} \right] \eta_x + \left[\beta UV - \tilde{\nu}\left(\frac{\partial U}{\partial y} + \frac{\partial V}{\partial x} \right) \right] \eta_y \right\} dS_e$$

where

$$\frac{\partial c_f}{\partial H} = \begin{cases} 0 \text{ , } \textit{if Chezy discharge coefficents are used} \\ \dfrac{\Phi g n^2}{H^{4/3}} \text{ , } \textit{if Manning roughness coefficients are used} \end{cases} \qquad (2\text{-}26)$$

and

Φ = 0.151 for U.S. customary units, or 0.333 for SI units

Derivative expressions for the residual of the conservation of momentum equation in the y direction are:

$$\frac{\partial f_{V_i}}{\partial U_j} \equiv \sum_e \int_{A_e} \left\{ N_i N_j \left[\Omega H + \frac{\tau_{by}}{\rho} \frac{U}{U^2 + V^2} \right] + \frac{\partial N_i}{\partial x} N_j [-\beta HV] + \frac{\partial N_i}{\partial x}\frac{\partial N_j}{\partial y}[\tilde{\nu}H] \right\} dA_e$$
$$+ \sum_e \int_{S_e} \left\{ N_i N_j \left[\beta HU\eta_y \right] - N_i \frac{\partial N_j}{\partial x}\left[\tilde{\nu}H\eta_y \right] \right\} dS_e \qquad (2\text{-}27)$$

$$\frac{\partial f_{V_i}}{\partial V_j} \equiv \sum_e \int_{A_e} \left\{ N_i N_j \left[\alpha H + \frac{\partial H}{\partial t} + \frac{\tau_{bx}}{\rho} \frac{2U^2 + V^2}{U(U^2 + V^2)} \right] \right.$$
$$\left. + \frac{\partial N_i}{\partial x} N_j [-\beta HU] + \frac{\partial N_i}{\partial x}\frac{\partial N_j}{\partial x}[2\tilde{\nu}H] + \frac{\partial N_i}{\partial y} N_j [-2\beta HV] + \frac{\partial N_i}{\partial y}\frac{\partial N_j}{\partial y}[\tilde{\nu}H] \right\} dA_e \qquad (2\text{-}28)$$
$$+ \sum_e \int_{S_e} \left\{ N_i N_j [2\beta HU\eta_x + \beta HV\eta_y] - N_i \frac{\partial N_j}{\partial x}[2\tilde{\nu}H\eta_x] - N_i \frac{\partial N_j}{\partial y}[\tilde{\nu}H\eta_x] \right\} dS_e$$

$$\frac{\partial f_{V_i}}{\partial H_j} \equiv \sum_e \int_{A_e} \left\{ N_i M_j \left[\alpha V + \frac{\partial V}{\partial t} + \Omega V + g \frac{\partial z_b}{\partial y} + \frac{\tau_{by}}{\rho c_f} \frac{\partial c_f}{\partial H} \right] \right.$$
$$+ \frac{\partial N_i}{\partial x} M_j \left[-\beta UV - gH + 2\tilde{\nu} \frac{\partial U}{\partial x} \right] + \frac{\partial N_i}{\partial y} M_j \left[-\beta UV + \tilde{\nu} \left(\frac{\partial U}{\partial y} + \frac{\partial V}{\partial x} \right) \right] \Bigg\} dA_e \qquad (2\text{-}29)$$
$$+ \sum_e \int_{S_e} \left\{ N_i M_j \left[\beta UU + gH + 2\tilde{\nu} \frac{\partial U}{\partial x} \right] \eta_x + \left[\beta UV - \tilde{\nu} \left(\frac{\partial U}{\partial y} + \frac{\partial V}{\partial x} \right) \right] \eta_y \right\} dS_e$$

The derivative expressions for the equation of continuity residuals are:

$$\frac{\partial f_{H_i}}{\partial U_j} = \sum_e \int_{A_e} \left\{ M_i \frac{\partial N_j}{\partial x} [H] + M_i N_j \left[\frac{\partial H}{\partial x} \right] \right\} dA_e - \frac{\partial Q_i}{\partial U_j} \qquad (2\text{-}30)$$

$$\frac{\partial f_{H_i}}{\partial V_j} = \sum_e \int_{A_e} \left\{ M_i \frac{\partial N_j}{\partial y} [H] + M_i N_j \left[\frac{\partial H}{\partial y} \right] \right\} dA_e - \frac{\partial Q_i}{\partial V_j} \qquad (2\text{-}31)$$

$$\frac{\partial f_{H_i}}{\partial H_j} = \sum_e \int_{A_e} \left\{ M_i \frac{\partial M_j}{\partial x} \left[\alpha + \frac{\partial U}{\partial x} + \frac{\partial V}{\partial y} \right] + M_i \frac{\partial M_j}{\partial x} [U] + M_i \frac{\partial M_j}{\partial x} [V] \right\} dA_e - \frac{\partial Q_i}{\partial H_j} \qquad (2\text{-}32)$$

Boundary Conditions

A physical region modeled in a surface water flow problem will have either closed, or no flux boundaries, or open boundaries. These boundary conditions are shown in Figure 4, Open and Closed Boundaries. The type of boundary and the flow condition will determine the needed boundary information.

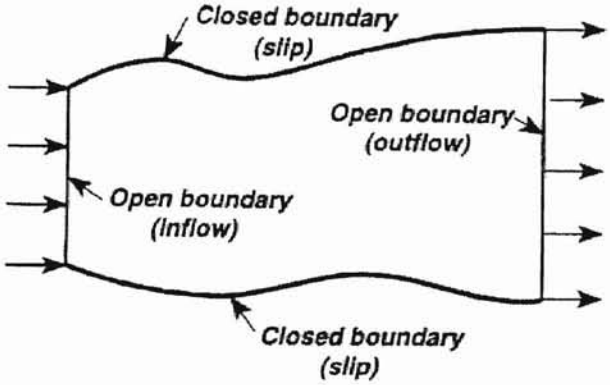

Figure 4. Open and Closed Boundaries [Source: Froehlich, 1996, p. 4-15]

Boundary conditions are specified around the perimeter of the area being modeled for the entire duration of the simulation. Boundary condition specification consist of either the normal flow or the normal stress, in addition to either the tangential flow or the tangential shear stress at all points on the boundary. The types and combinations of possible boundary conditions which may be specified are given in Table I, Possible Boundary Specifications for Various Flow Conditions and Boundary Types.

A closed boundary defines a geometric feature such as a natural shoreline, an embankment, a jetty, or a seawall. Flow across a closed boundary generally equals zero. An open boundary defines an area along the boundary of a finite element network where flow is allowed to enter or leave the network.

The Galerkin finite element formulation allows complex conditions to be automatically satisfied as natural conditions of the problem. These natural boundary conditions are implicitly impressed in the problem statement and require no further treatment. Those boundary conditions imposed explicitly are known as forced, or essential, conditions. These boundary values are prescribed by modifying the finite

element equation governing that variable. Additionally, special boundary conditions imposed by one dimensional flow can also be applied.

TABLE I

POSSIBLE BOUNDARY SPECIFICATIONS[a] FOR VARIOUS FLOW CONDITIONS AND BOUNDARY TYPES. (FROEHLICH, 1996, P. 4-18)

Type of boundary	Flow condition	
	Subcritical	Supercritical
Closed, $U_n = 0$	$U_n = U_n^*$ (usually $U_n^* = 0$)	
Inflow, $U_n < 0$	$U_n = U_n^*$ and $U_t = U_t^*$, or $q_n = q_n^*$ and $q_t = q_t^*$, or $H = H^*$ and $U_t = U_t^*$, or $H = H^*$ and $q_t = q_t^*$ (usually $U_t = q_t = 0$).	$U_n = U_n^*$, $U_t = U_t^*$, and $H = H^*$, or $q_n = q_n^*$, $q_t = q_t^*$, and $H = H^*$ (usually $U_t = q_t = 0$).
Outflow, $U_n > 0$	$H = H^*$	nothing
Weakly-reflecting	$-U_n + 2\sqrt{gH} = -U_{n-} + 2\sqrt{gH_-}$	

[a] U_n = outward normal velocity, U_t = tangential velocity, $q_n = U_nH$ = outward normal unit flow rate, $q_t = U_tH$ = tangential unit flow rate, U_{n-} = outward normal velocity in a fictitious river far upstream from the boundary, H_- = depth in a fictitious river far upstream from the boundary.

CHAPTER III

SCOUR EQUATIONS

General

Scour is the result of the erosive forces of flowing streams. These forces carry material from one area of the stream downstream to another area of the stream. Scour, such as occurs at highway bridge crossings, is generally differentiated from general bed degradation and plan changes in a river as being localized in nature.

Obviously, different materials will scour at different rates. Loose, uncemented materials such as sand, may scour quickly in rapidly flowing water. Cemented soils, such as clays, may scour much more slowly. However, Richardson, Harrison, Richardson, and Davis (1993) state that the ultimate scour in cohesive or cemented soils can be as deep as scour in sand bed streams. Foundations placed in massive homogeneous rock formations are likely to be highly resistant to scour during the lifetime of a highway bridge.

Many different researchers have developed equations for predicting contraction and local scour. All of these equations are based upon theoretical assumptions and laboratory experiments with little or no field verification. Additionally, many of these equations do not account for site specific or subsurface conditions.

Total Scour

Total Scour at a highway bridge is generally considered to be made up of three components. All three of these components together comprise the total scour at a

highway bridge. These are:

1. Aggradation and Degradation
2. Contraction Scour
3. Local Scour

In addition to the three types of scour mentioned above lateral, shifting of the stream within its floodplain can often damage a highway bridge.

Aggradation and Degradation

Aggradation and degradation, sometimes referred to as gradation changes, refer to long term, general changes of the slope and elevation of the stream bed. These changes generally occur over a large segment of the stream. Aggradation involves the raising of the stream bed as a result of deposition of sediment. Degradation involves the lowering of the stream bed as a result of the removal of sediment.

Gradation changes can be caused by both natural and man made factors. Some of the man made factors which can cause these changes are: channel alterations, stream bed mining, construction of dams and reservoirs, and land use changes. Natural causes of stream gradient instability are primarily natural channel alterations, earthquake, tectonic and volcanic activities, climatic changes, fire and channel bed and bank material erodibility. Additionally, a long term trend in bed elevation may change over the life of a highway structure.

The long term stability of a stream can be described by the sediment continuity concept. According to Lagasse, Schall, Johnson, Richardson, Richardson and Chang (1991) the sediment inflow minus the sediment outflow equals the time rate of change of

sediment volume in a given reach. In simpler terms this means that the amount of sediment entering a reach minus the amount of sediment leaving that same reach equals the change in the amount of sediment stored in that reach of the stream. This concept is demonstrated in Figure 5, Definition Sketch of Sediment Continuity Concept Applied to a Given Channel Reach Over a Given Time Period.

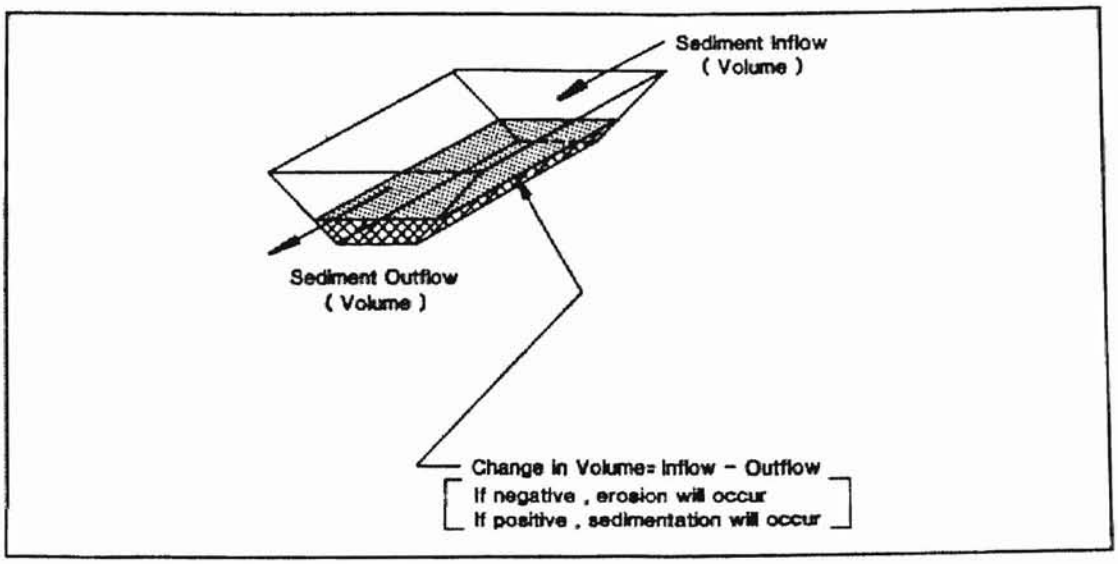

Figure 5. Definition Sketch of Sediment Continuity Concept Applied to a Given Channel Reach Over a Given Time Period [Source: Lagasse et al., 1991, p. 28]

The problem facing the engineer is to predict the change in the stream bed elevation which will occur over the life of a highway structure. A quantitative estimate of change in the stream bed elevations can be made by using the Federal Highway Administrations *HEC-20 Stream Stability at Highway Structures*. A sediment continuity computer program such as BRI-STARS or the Corps of Engineers HEC-6 can be used to make a quantitative estimate of the change in the stream bed elevation. Also, data documenting the long term changes in stream bed elevations is available from the U.S. Army Corps of Engineers and other agencies.

Contraction Scour

General Contraction Scour occurs at bridges because the flow area of the stream is reduced by either a natural decrease in flow area or by abutments or piers blocking a portion of the flow area. This reduction in waterway area results in an increase in velocity at the bridge. Increased velocity results in an increase in shear stress which causes the removal of sediment from the area of the bridge. This removal of sediment results in a lowering of the natural stream elevation and a subsequent increase in the stream cross section. This increase of the stream cross section continues, in the riverine situation, until the velocity and shear stress are reduced to a point where equilibrium is reached.

There are two types of contraction scour. Live-bed scour occurs when there is sediment being transported into the constricted channel section from the unconstricted area upstream. Clear-water scour occurs when there is negligible transport of sediment from the unconstricted section to the constricted sections. Typically, both types of scour are cyclic. That is, scour increases during the rising stage of a runoff event and fills at least partially on the falling stage.

Contraction scour equations are based upon the principle of conservation of sediment transport. In the case of live-bed scour, maximum scour occurs when the shear stress reduces to the point that the sediment transported into the constricted section equals the sediment transported out of the constricted section. At this point the conditions for sediment continuity are in balance. During clear-water scour the maximum scour occurs when the shear stress reduces to the critical shear stress of the material.

Contraction scour will also depend upon whether the bridge is a relief bridge or a

bridge over a main channel. According to Laursen (1963) a secondary bridge placed on the floodplain will divert a part of the flow from the main channel crossing: the "relief" thus obtained presumably permits a reduction in the length of the bridge over the main channel and in the height of fills. Therefore, to calculate contraction scour at a bridge it is necessary to determine if the flow upstream of the bridge is transporting sediment or not and whether the bridge is a relief bridge or a bridge over the main channel.

Live Bed Contraction Scour Laursen (1960) derived a clear-water contraction scour equation based upon a long contraction and a simplified transport function. Richardson et al. (1993) presented Laursen's equation as:

$$\frac{y_2}{y_1} = \left(\frac{Q_2}{Q_1}\right)^{\frac{6}{7}} \left(\frac{W_1}{W_2}\right)^{K_1} \left(\frac{n_2}{n_1}\right)^{K_1} \qquad (3\text{-}1)$$

where

y_1 = average depth in upstream channel, in feet

y_2 = average depth in contracted section, in feet

W_1 = bottom width of upstream main channel, in feet

W_2 = bottom width of main channel in the contracted section, in feet

Q_1 = flow in the upstream channel transporting sediments, in cubic feet per second

Q_2 = flow in the contracted channel, in cubic feet per second

n_1 = Manning's n for the upstream main channel

n_2 = Manning's n for the contracted section

K_1 and K_2 = exponents determined from Table II below, based upon the mode of material bed transport

TABLE II

VALUE OF k_1 AND k_2

V_o / w	K_1	K_2	Mode of Bed Material Transport
<0.50	0.59	0.066	Mostly contact bed material
0.50 to 2.0	0.64	0.21	Some suspended bed material discharge
>2.0	0.69	0.37	Mostly suspended bed material discharge

in Table II

$V_o = (g\ y_1\ S_1)^{1/2}$ shear velocity in the upstream section, in feet per second

s_1 = slope of energy grade line of main channel, in feet per feet

D_{50} = median diameter of the bed material, in feet

$_w$ = median fall velocity of the bed material based upon the D_{50}, see Figure 6

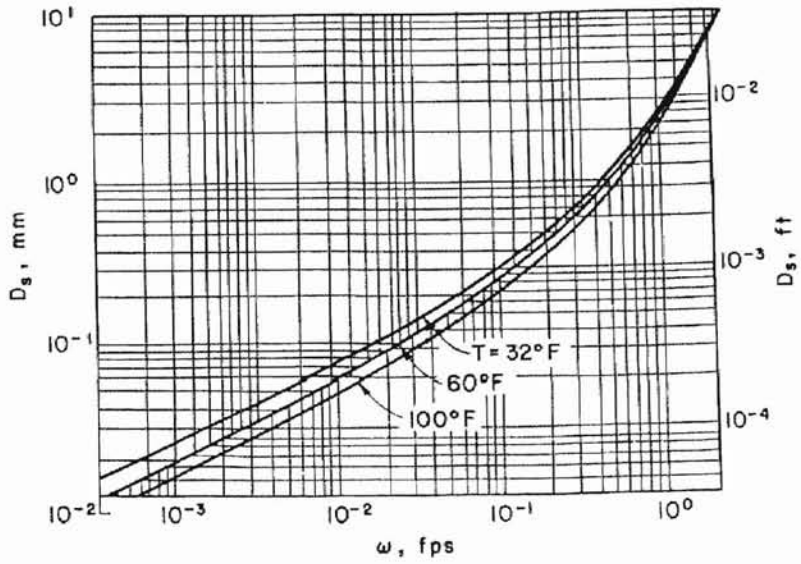

Figure 6. Fall Velocity of Sand Sized Particles [Source: Richardson et al., 1993, p. 34]

In Equation 3-1 the material scoured during a flood is deposited over a large area so that:

$$y_s = y_2 - y_1 \tag{3-2}$$

where

y_s = average scour depth, in feet

Clear-Water Contraction Scour Laursen (1963) also presented an equation commonly used to predict clear-water scour. This equation is based upon the assumption, stated earlier, that clear-water scour is the greatest when the shear stress in the contracted section equals the critical shear stress, or as:

$$\tau_2 = \tau_c \tag{3-3}$$

where

τ_2 = average bed shear stress in the contracted section, in pounds per square foot

τ_c = critical bed shear stress at incipient motion, in pounds per square foot

The shear stress may be stated in terms of the Manning's equation as:

$$\tau_2 = \gamma\, y_2\, S_f = \frac{\gamma\, V_2^{\,2}\, n^2}{(1.49)^2\, y_2^{\,1/3}} \tag{3-4}$$

where

γ = the unit weight of water, 62.4 pounds per cubic foot

S_f = slope of the energy grade line, in feet per foot

V_2 = average velocity in the contracted section, in feet per second

Richardson et al. (1993) make use of the previous relationships, Stricklers's approximation and continuity to present Laursen's clear-water contraction scour equations as:

$$\frac{y_2}{y_1} = \left(\frac{W_1}{W_2}\right)^{\frac{6}{7}} \left[\frac{V_1^2}{120\, y_1^{\frac{1}{3}}\, D_{50}^{\frac{2}{3}}}\right]^{\frac{3}{7}} \tag{3-5}$$

where

V_1 = average velocity in the upstream main channel; in feet per second

and again:

$$y_s = y_2 - y_1 \tag{3-6}$$

Froehlich (1996) presented equation 3-4 in terms of SI units and two-dimensional flow as:

$$d_{sc} = \left[\frac{\rho\, g\, n^2\, q^2}{\tau_c}\right]^{3/7} - H \tag{3-7}$$

where,

d_{sc} = clear-water contraction scour depth

ρ = density of water

H = water depth

and

$$q = H\sqrt{U^2+V^2} = \textit{unit flow rate} \tag{3-8}$$

where

U and V = depth-averaged velocities in the x and y directions respectively

Local Scour

Local scour is the result of the formation of vortices caused by obstructions to the flow. In the case of a highway bridge the flow obstruction can be either a pier or abutment. These obstructions accelerate the flow in their immediate area and create vortices that remove the material around them. Local scour, like contraction scour, may be either clear-water or live-bed scour.

Pier Scour As mentioned previously, a bridge pier will cause a system of vortices which are responsible for local scour. These vortex systems are well understood and are described in detail by Molinas (1990) and Chiew (1992). Depending upon the bridge pier and the flow conditions the vortex system will be made up of a horseshoe-vortex, a wake-vortex, and a trailing vortex. These vortex systems are shown in Figure 7, Flow Pattern at a Cylindrical Pier.

As shown in Figure 7, the vertical velocity distribution in an open channel is characterized by the no slip condition at the bottom of the channel. As flow approaches a pier a stagnation plane is formed on the upstream face of the pier. That is the flow velocity in a vertical plane, approaches zero on the upstream face of the pier. Because of the vertical velocity profile a downward pressure gradient, and therefore downward flow, are formed on the upstream face of the pier. This downward flow will cause a three-dimensional separation of the boundary layer which rolls up ahead of the pier creating a horseshoe-vortex system. The horseshoe-vortex system is very efficient at dislodging and

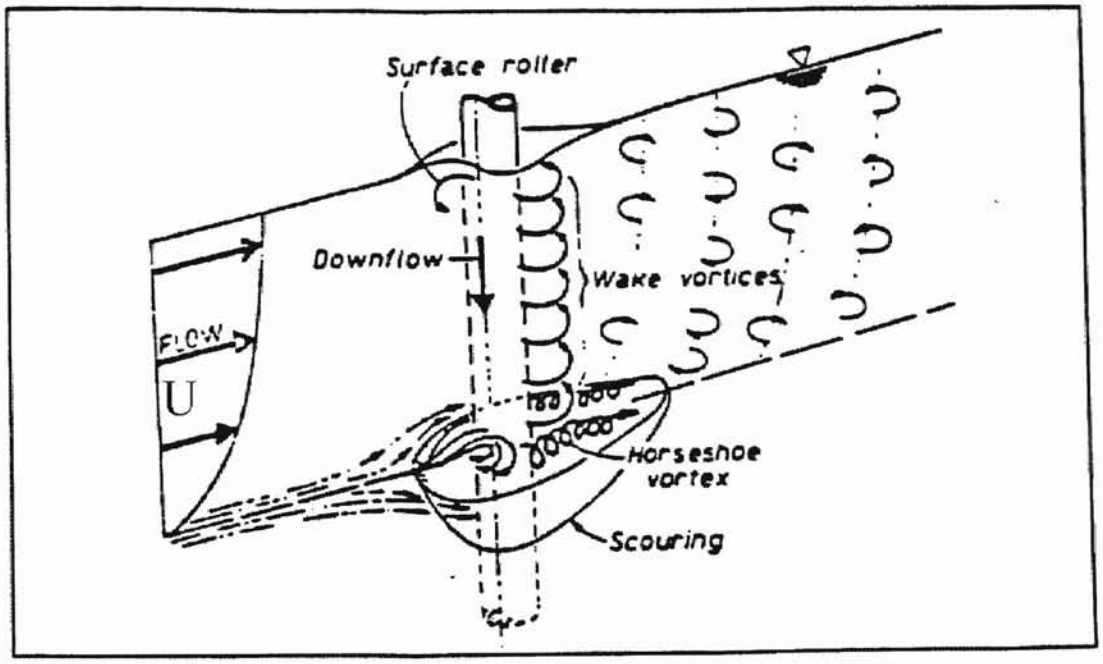

Figure 7. Flow Pattern at a Cylindrical Pier [Molinas, 1990, p.31]

removing soil particles from the base of the pier, therefore, causing local scour.

The formation of a stagnation plane on the upstream face of the pier also causes a lateral acceleration of flow past the pier. This acceleration causes the formation of vertical vortices downstream of the pier which are referred to as the wake-vortex. This vortex system also causes removal sediment from the base of the pier. A blunt-nosed pier will cause the formation of a strong wake vortex system, whereas, a more streamlined pier shape, referred to as a sharp-nosed pier, will create a weaker vortex system.

A trailing-vortex system is composed of one or more discrete vortices beginning at the top of the pier and extending downstream. These vortices are created when a finite pressure difference exists between two flow surfaces moving at a corner. This type of vortex system usually only occurs on a completely submerged pier.

Figure 8, Scour Depth for a Given Pier & Sediment Size as a Function of Time &

Approach Velocity, describes the progression of pier scour as a function of time and approach velocity for a given pier and sediment size. Clear-water scour will cease when the shear stress caused by the horseshoe-vortex systems equals the critical shear stress of the sediment particles at the bottom of the hole. Live-bed scour will fluctuate about an equilibrium scour depth in response to the formation of varying bed forms. This equilibrium scour depth will be reached when the amount of sediment leaving the scour hole is equal to the amount of sediment supplied to the scour hole.

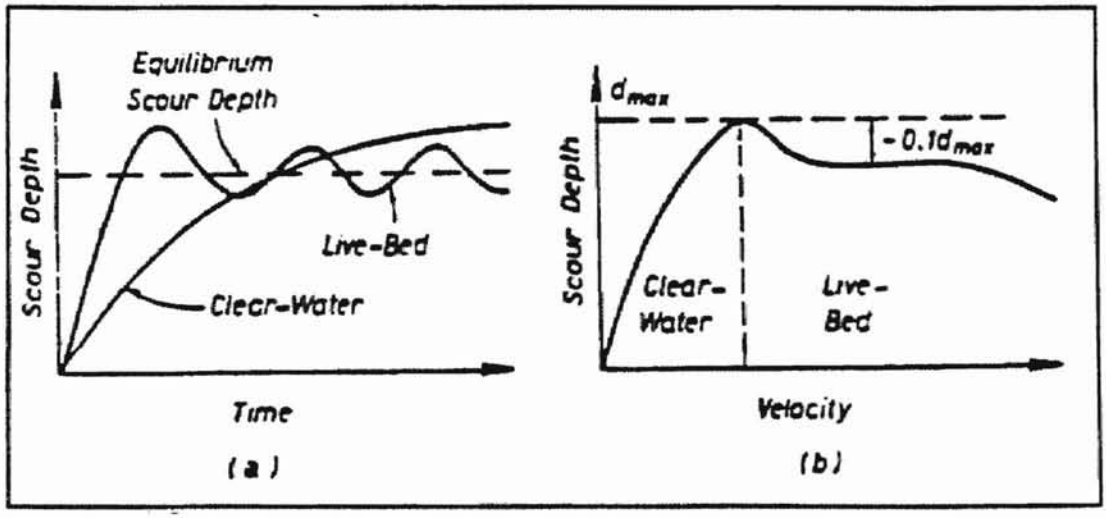

Figure 8. Scour Depth for a Given Pier and Sediment Size as a Function of Time and Approach Velocity. [Molinas, 1990, p.30]

According to Molinas (1990) and Richardson et al. (1993) the following factors influence scour around bridge piers:

1. Pier shape, width, orientation, and presence of ice and debris.
2. Approach flow depth and velocity.
3. Bed configuration and sediment diameter and density.
4. Density and kinematic viscosity of the fluid.

By incorporating the above parameters several researchers have developed equations to predict local scour at bridge piers. Most of these equations have been based on laboratory tests and many yield different estimates of scour depth for a given set of scour data.

Richardson et al. (1993) presented Figure 9, Comparision of Scour Formulas for Variable Depth Ratios (y/a) and Figure 10, Comparison of Scour Formulas with Field Scour Measurements, which were prepared by the Federal Highway Administration and compare many of the more common scour equations. Both Molinas (1990) and Becker (1994) presented several of the more commonly used scour equations.

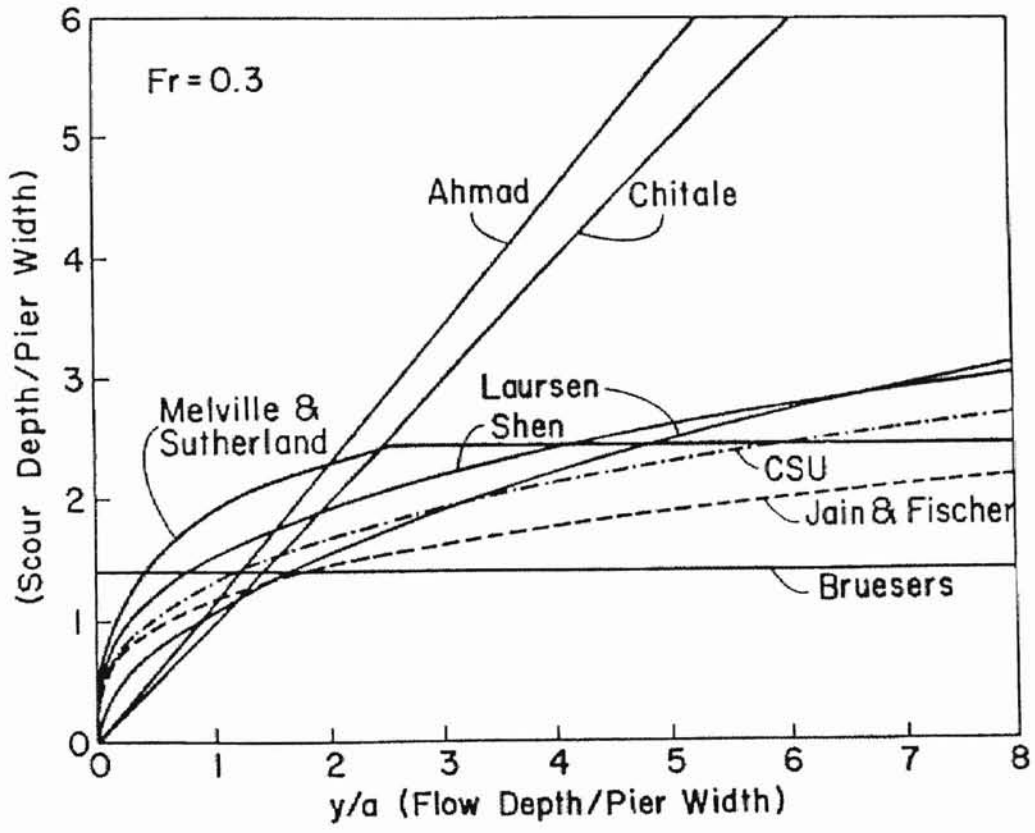

Figure 9. Comparison of Scour Formulas for Variable Depth Ratios (y/a) [Source: Richardson et al., 1993, p.37]

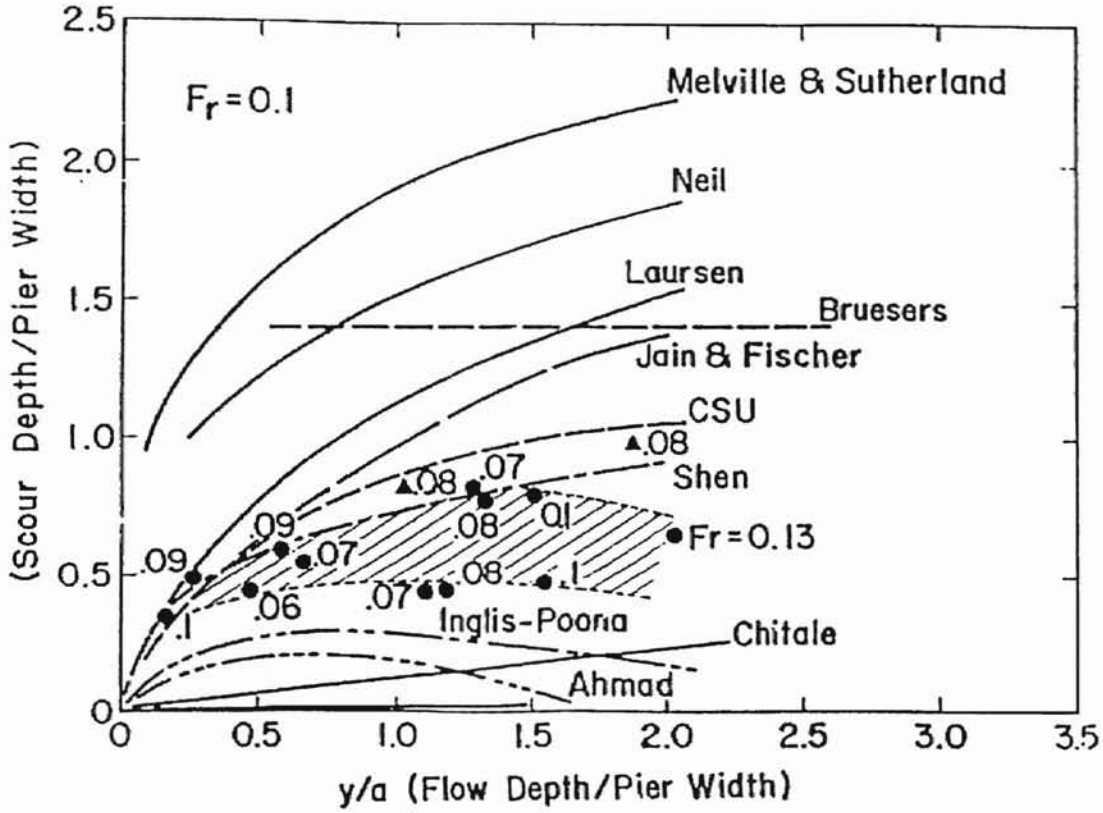

Figure 10. Comparison of Scour Formulas with Field Scour Measurements. [Source: Richardson et al., 1993, p.37]

As can be seen from Figure 10 the Colorado State University Equation envelopes all of the data points, but gives lower values than many of the other equations. Therefore, the Colorado State University Equation is recommended by Richardson and others (1993) for use in predicting pier scour. Richardson and others (1993) presented the Colorado State University equation for pier scour as:

$$\frac{y_s}{q} = 2.0\ K_1\ K_2\ K_3\ \left(\frac{y_1}{a}\right)^{0.35}\ Fr_1^{0.43} \qquad (3\text{-}9)$$

where

y_s = scour depth, in feet

a = pier width, in feet

K_1 = a coefficient based on pier nose shape, 1.1 for square nosed piers, 0.9 for sharp nosed piers, 1.0 for round or circular nosed piers and 1.0 for a group of cylinders

K_2 = correction factor for angle of attack of flow from Table III

K_3 = correction factor for bed condition from Table IV

y_1 = flow depth directly upstream of pier, in feet

Fr_1 = Froude Number = $V_1 / (gy_1)^{1/2}$

V_1 = mean velocity of flow directly upstream of the pier, in feet per second

TABLE III

CORRECTION FACTOR K_2 FOR ANGLE OF ATTACK OF THE FLOW
[Souce: Richardson et al., 1993, p. 40]

Angle	$L/a_1 = 4$	$L/a = 8$	$L/a = 12$
0	1.0	1.0	1.0
15	1.5	2.0	2.5
30	2.0	2.5	3.5
45	2.3	3.3	4.3
90	2.5	3.9	5.0

Angle = skew angle of flow
L = length of pier

TABLE IV

INCREASE IN EQUILIBRIUM PIER SCOUR DEPTHS K_3
FOR BED CONDITION
[Source: Richardson et al., 1993, p. 40]

Bed Condition	Dune Height H (ft)	K_3
Clear Water Scour	N/A	1.1
Plane Bed & Antidune Flow	N/A	1.1
Small Dunes	10>H>2	1.1
Medium Dunes	30>H>10	1.1 to 1.2
Large Dunes	H>3	1.3

Debris lodged on piers have the effect of increasing local scour at a pier. This occurs because the effective pier width is increased and a greater amount of the flow is directed downward. However, increasing flow depth tends to decrease the effect of debris on piers. Melville and Dongal (1992) have made recommendations concerning the treatment of debris on piers.

Abutment Scour The mechanism of local scour at abutments is identical to that at piers. The same system of vortices is formed. These vortices, as at piers, remove sediment from the stream bed in the vicinity of the abutment. Therefore, the same considerations apply to abutment scour, as apply to pier scour.

As with the pier scour many equations have been developed to predict local scour at abutments. These equations are based entirely upon laboratory data and tend to predict excessively conservative scour depths for the field situation. This happens because the

length of the abutment obstructing flow is easily measured in the laboratory, whereas, in the field this value proves to be more elusive. Another problem is that little field data on abutment scour exists.

Melville (1992) presented a procedure to calculate abutment scour based upon laboratory data. This procedure accounts for abutment length, flow depth, and abutment shape and alignment. The procedure presents equations in terms of the abutment length to flow depth. In summary the abutment scour equations are:

$$d_s = 2\ K_s\ L \qquad \frac{L}{y} < 1 \tag{3-10}$$

$$d_s = 2\ K_s^*\ K_\theta^*\ (yL)^{0.5} \qquad 1 \le \frac{L}{y} \le 25 \tag{3-11}$$

$$d_s = 10\ K_\theta\ y \qquad \frac{L}{y} > 25 \tag{3-12}$$

where

d_s = depth of scour, in feet

K_s = shape factor from Table V

K_θ = factor accounting for abutment alignment from Figure 11

L = length of the abutment including the bridge approach measured perpendicular to flow

y = flow depth in feet

The factor K_s accounts for abutment shape. However, as the abutment and bridge approach become longer the effect of abutment shape diminishes. Therefore, the value K_s should be adjusted as follows:

$$K_s^* = K_s \qquad \frac{L}{y} \leq 10 \tag{3-13}$$

$$K_s^* = K_s + (1 - K_s)\,(0.1\frac{L}{y} - 1.5) \qquad 10 < \frac{L}{y} < 25 \tag{3-14}$$

$$K_s^* = 1 \qquad \frac{L}{y} \geq 25 \tag{3-15}$$

TABLE V

SHAPE FACTORS [Melville, 1992, p. 617]

Abutment Shape (1)	Shape Factor, K_s (2)
Vertical plate or narrow vertical wall	1.0
Vertical wall abutment with semicircular end	0.75
45° wing wall	0.75
Spill-through (H : V):	
0.5 : 1	0.60
1 : 1	0.50
1.5 : 1	0.45

The factor K_θ accounts for abutment alignment. However, the effect of abutment alignment diminishes as the abutment and bridge approach become shorter. Therefore, the value K_θ should be adjusted as follows:

$$K_\theta^* = K_\theta \qquad \frac{L}{y} \geq 3 \tag{3-16}$$

$$K_\theta^* = K_\theta + (1 - K_\theta)\,(1.5 - 0.5\,\frac{L}{y}) \qquad 1 < \frac{L}{y} < 3 \tag{3-17}$$

$$K_\theta^* = 1 \qquad \frac{L}{y} \leq 1 \tag{3-18}$$

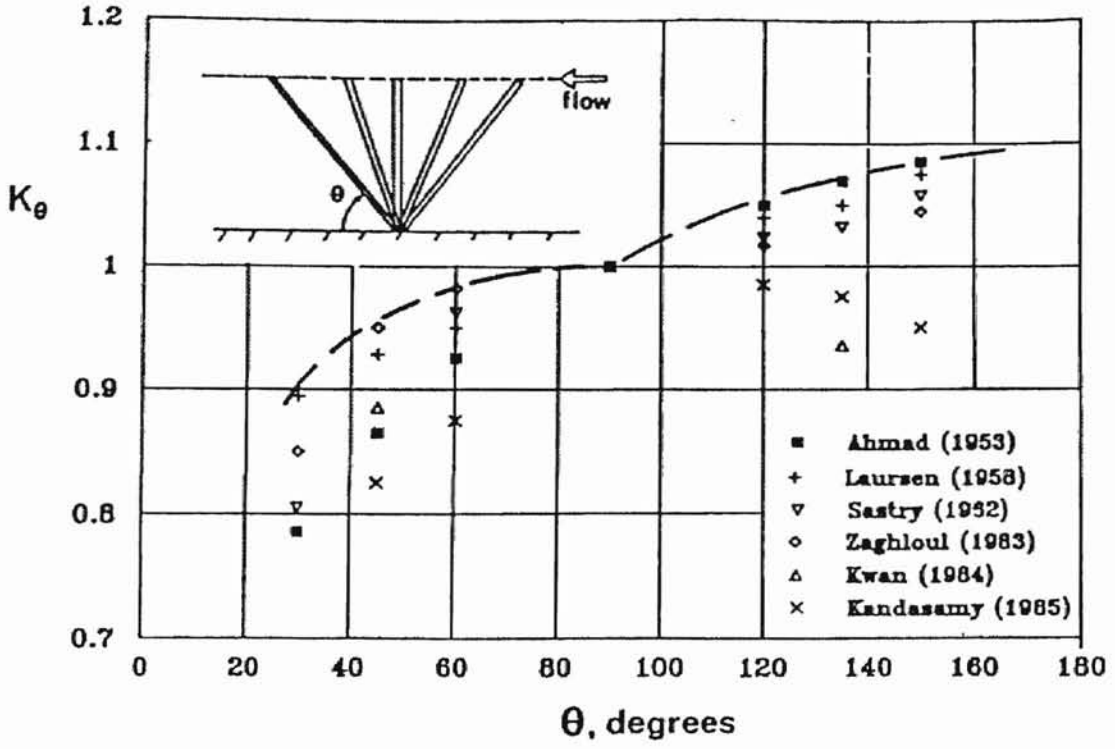

Figure 11. Influence of Abutment Alignment of Scour Depth [Source: Melville, 1992, p. 623]

Clear-Water and Live Bed Scour

As mentioned previously both clear-water, and live-bed scour can occur during contraction and local scour. Clear-water scour occurs when there is no movement of the bed material upstream of the crossing. However, in this case, the acceleration of flow and

vortices created by local obstructions cause scour. Live-bed scour occurs when the bed material upstream of the crossing is moving.

Richardson et al. (1993) suggested using Neill's equation for determining the velocity associated with the initiation of movement to determine if either clear-water or live-bed scour is occurring. This equation is:

$$V_c = 1.58\ [(S_s - 1)\ g\ D_{50}]^{\frac{1}{2}} \tag{3-19}$$

where

V_c = the critical velocity above which bed material of a size D_{50} and smaller will be transported, in feet per second

S_s = the specific gravity of the bed material

A value of 2.65 is common for most bed material. Therefore, Equation 3-19 reduces to:

$$V_c = 11.52\ y^{\frac{1}{6}}\ D_{50}^{\frac{1}{3}} \tag{3-20}$$

Also according to Richardson et al. (1993) Laursen presented this equation as:

$$V_c = 10.95\ y^{\frac{1}{6}}\ D_{50}^{\frac{1}{3}} \tag{3-21}$$

The only difference between these two equations are the coefficients 11.52 and 10.95. Realistically either equation can be used to decide whether clear-water or live-bed scour will occur.

CHAPTER IV

METHODOLOGY AND APPLICATION

Modeling Systems Operations

The following steps are generally followed in any hydraulic or numerical modeling application:

1. Data collection
2. Network design
3. Model calibration
4. Model testing
5. Model application

Therefore, these steps should also be followed in the application of the FESWMS-2DH computer model.

After a surface water flow problem has been defined, the first step in the construction of a hydraulic model consists of gathering adequate topographic and hydraulic data. This data might include things such as topographic maps, aerial photos, and gage records. When applying the FESWMS-2DH computer model network design is accomplished by subdividing the area being modeled into an assemblage of finite elements. The goal of network design is to create a representation of the area being modeled that provides an adequate approximation of the true solution of the governing equations at a reasonable cost.

The FESWMS-2DH computer program provides a numerical approximation to complex surface water flow problems. This is accomplished by describing the physics of

surface water flow in a series of equations in which several empirical coefficients appear. Therefore, when enough data are available, the dimensions of the simplified geometric elements and empirical hydraulic coefficients need to be adjusted so that values computed by the model reproduce as closely as possible measured values. This process is referred to as model calibration.

Model testing is accomplished by applying a calibrated model to other flow situations for which measured values are available. This is an important, but not always possible step. If a model reproduces reasonable results on flow conditions outside the range of which it was calibrated, it can be used to simulate conditions outside of that range with more confidence than if no testing were carried out.

Model application consists of applying the model to simulate a variety of flow conditions. Model application is only attempted after the previous steps have been carried out in one form or another. Models still need to be applied carefully, especially to model conditions outside of the range for which they were calibrated. However, a well constructed, calibrated and tested model can be used to answer a variety of surface water flow problems.

Site Overview

Description of Site

As mentioned previously, prior to 1988, the Interstate-35 and Cimarron River crossing consisted of two main bridges and a series of eight overflow bridges all placed in a parallel arrangement. This arrangement utilized a main structure over the river channel and four groups of overflow bridges on the floodplain. The overflow structures were

placed at increments of 900 feet, 450 feet, and 650 feet apart. The flowline of the main bridges were approximately 870.2 feet while the flowlines of the overflow bridges ranged from 885 feet to 887 feet. This arrangement is shown in Figure 12, Interstate-35 and the Cimarron River Site Plan. Additional information concerning the length and elevation of each bridge is given below in Table VI, Bridge Dimensions. A portion of the United States Geological Survey quadrangle map describing the site is included in Appendix A.

TABLE VI

BRIDGE DIMENSIONS

Bridge	Length	Floor Elevation (feet)	Low Steel Elevation (feet)
Main Bridge (Left)	805' 9 3/4"		916.9
Main Bridge (Right)	805' 9 3/4"		905.9
Overflow 1 & 2	282' 6"	904.7	901.4
Overflow 3 & 4	200' 6"	904.8	901.5
Overflow 5 & 6	280' 6"	904.9	901.5
Overflow 7 & 8	160' 6"	904.8	901.4

According to Yalin (1992) a stream may be considered as meandering when the deformation of a meandering stream exhibits a traceable periodicity along the general flow direction and this deformation is induced by the stream itself: it should not be "forced" upon the stream by its environment. Meandering is a phenomena which happens to many mature streams and is not fully understood. Further, according to Strongylis (1988), comparison of aerial photos of the site taken in 1937, 1939, 1957 and 1990 reveals that the Cimarron River exhibits a fair degree of meandering. Currently, and in

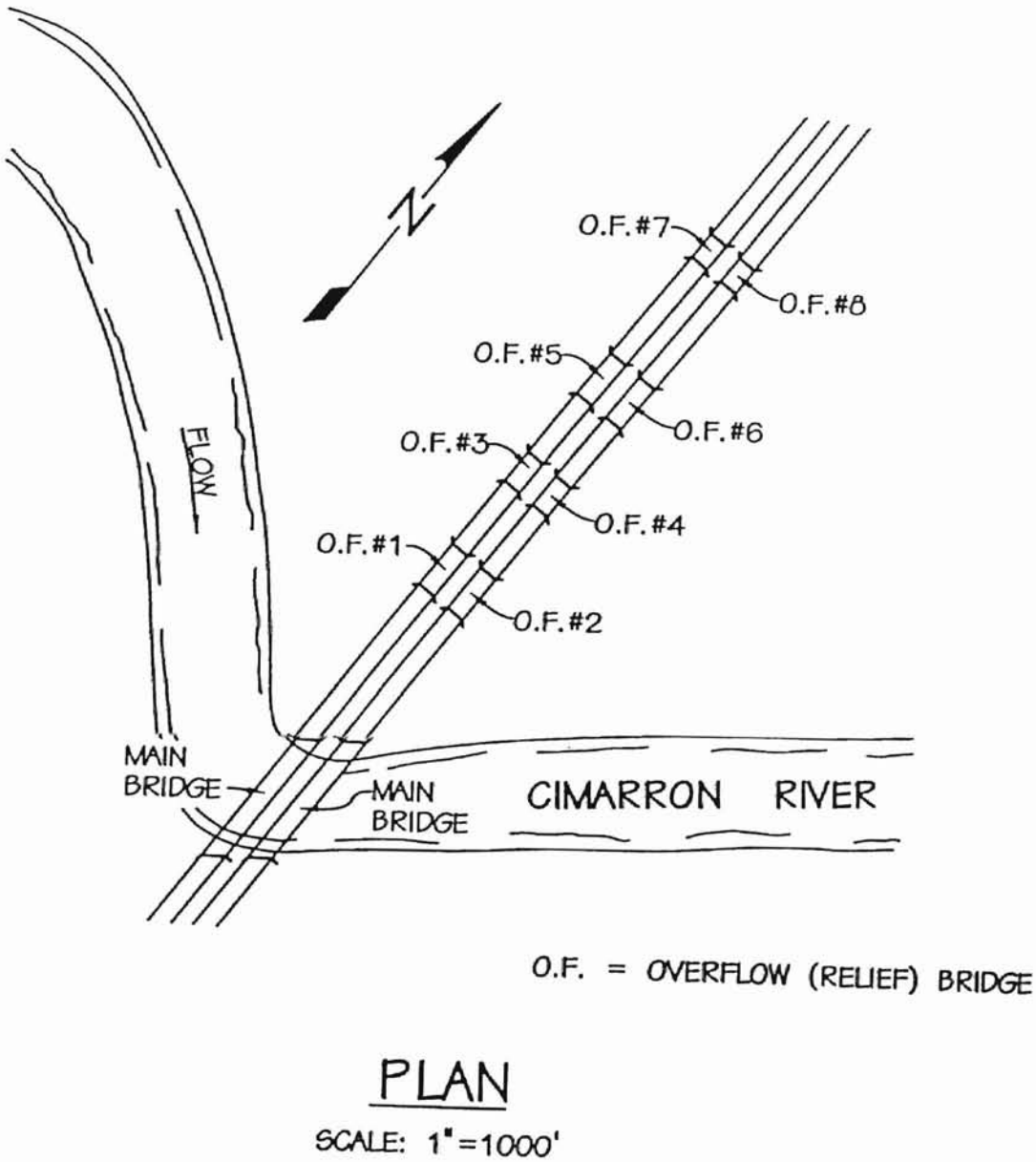

Figure 12. Interstate-35 and the Cimarron River Site Plan

1987, the main channel crosses under the main bridge on the south side of the floodplain. However, immediately before crossing under the bridge the channel makes a sharp curve to go from running perpendicular to the axis of the floodplain to crossing underneath the main bridge parallel to the axis of the flood plain. This occurs because over the years the meander curves in the river have moved downstream to the immediate vicinity of the bridge.

Hydrologic Data

As mentioned previously a large flood passed under these previously existing bridges in October of 1986. This flood caused a large amount of scour damage especially to the overflow bridges which led to the replacement of the previously existing bridges in 1987. Information describing this event was available from Oklahoma Department of Transportation study files and photographs.

The O.D.O.T. study files contained information concerning not only the Interstate-35 and Cimarron River crossing, but also data from the United States Geological Survey gage number 07161000. This gage is located at Perkins , Oklahoma, approximately 17 miles downstream of the Cimarron River crossing. By projecting the data from this gage upstream a flow rate of 156,000 cubic feet per second, approximately a Q_{52} event, was determined for the Cimarron River crossing for the October 1986 flood. Additionally, the water surface approximately 5000 feet downstream of the main bridge was determined to be 898.0 feet for the same event. This downstream water surface corresponded to a water surface upstream of the bridges of approximately 900.95 feet, which would indicate a lack of pressure flow at the overflow bridges.

In 1987, while designing the existing bridges, the Hydraulics Branch of the O.D.O.T. Bridge Division developed discharge information for this site. This was accomplished by using existing gage data and performing a statistical analysis using Log-Pearson Type III distribution. The results of this analysis are included in Appendix B and below.

Q_5 = 63,805 cfs

Q_{10} = 88,650 cfs

Q_{25} = 125,040 cfs

Q_{50} = 154,600 cfs

Q_{100} = 185,800 cfs

Q_{500} = 264,600 cfs

Soils Information

Soils information for the overflow bridges was taken from the *Soil Survey of Payne County Oklahoma* completed by the Soil Conservation Service of the U.S. Department of Agriculture. Applicable portions of this survey are included in Appendix C. Additional information was taken from the set of construction plans, completed by the O.D.O.T. in 1959, used to construct the previously existing bridges.

From the available soils information it was determined that the soil which was present below overflow bridges 1, 2, 3 and 4 had the soils name Yahola. This soil ranged in texture from a fine sandy loam near the surface to a stratified loam to loamy fine sand at a depth of approximately five feet. The soil which existed below overflow bridges 5, 6, 7 and 8 had the soils name Hawley. This soil ranged in texture from a fine sand loam

near the surface to a stratified loamy fine sand to silty clay loam at a depth of approximately five feet. The Cimarron River at this point has a wide floodplain and coarse sand in its bed.

From the construction plans, it was determined that the overflow bridge piers were 16 inch square piles driven to a layer of material labeled as "Red Bed". This material was present at an elevation of approximately 854.0 feet to 856.9 feet. The label "Red Bed" denotes a shale layer.

Recorded Scour Data

The October 1986 flood of the Cimarron River resulted in severe scour at all of the previously existing bridges. However, the damage was particularly severe at the eight overflow bridges. This occurred because a large amount of flow was directed through these structures and the meander located upstream of the bridges lead to skewed flow on the floodplain. Aerial photos of the scour holes taken from O.D.O.T. study files are shown in Figure 13, Aerial Photos of the Scour Holes at Interstate-35 and the Cimarron River. These photographs were taken on 11-11-86 approximately two weeks after the flood. A considerable amount of scour damage also occurred to the main bridges during this flood, however, in Figure 13 this damage is obscured by water in the main channel.

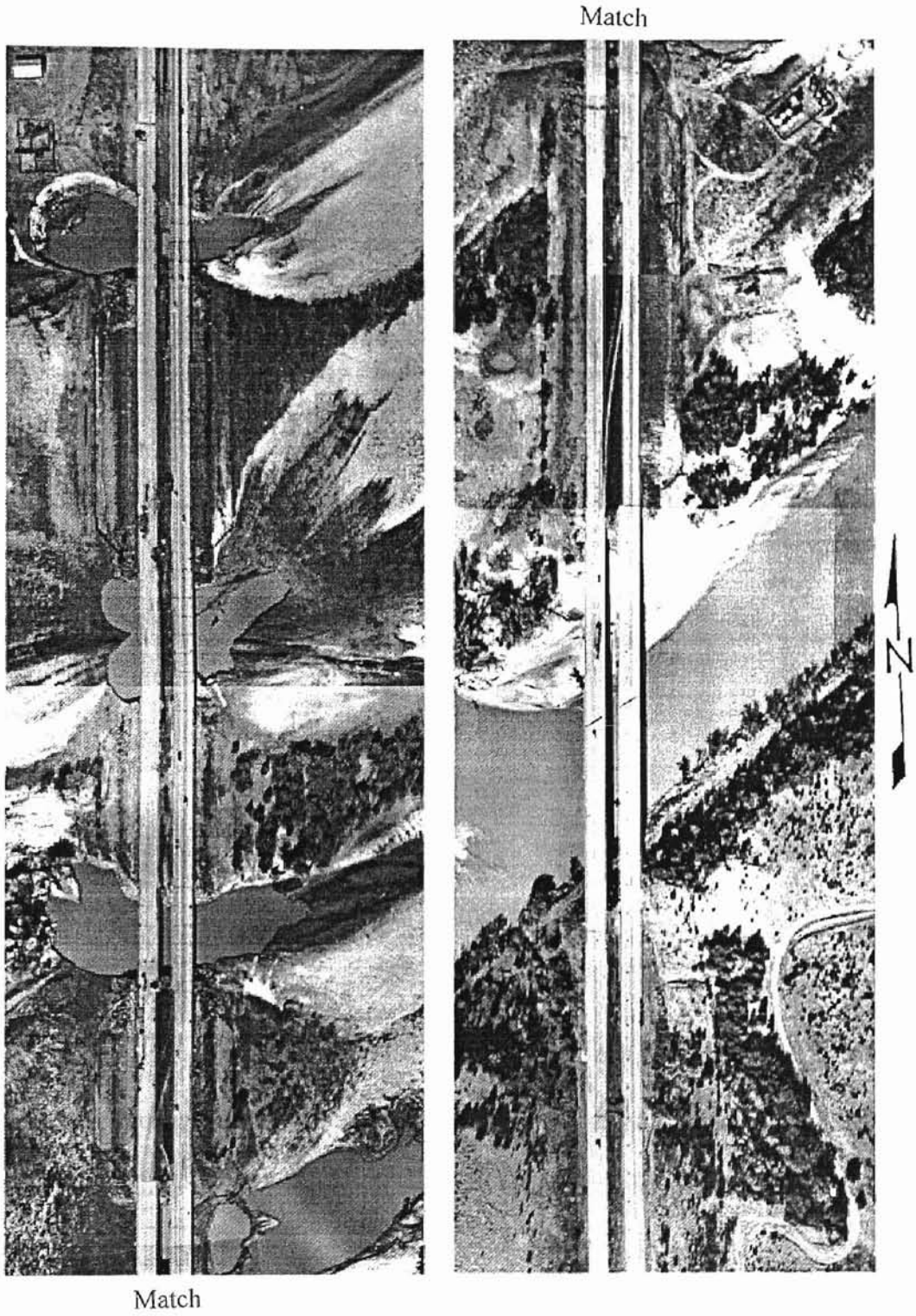

Figure 13. Aerial Photos of the Scour Holes at Interstate-35 and the Cimarron River

Tyagi (1988) presented a summary and analysis of the scour holes located at the eight overflow bridges. A summary of this study is presented in Table VII, Maximum Scour Depths Near Overflow Structures at the I-35 Bridge on the Cimarron River. Additional parts of this study are located in Appendix D.

TABLE VII

MAXIMUM SCOUR DEPTHS NEAR OVERFLOW STRUCTURES AT THE I-35 BRIDGE ON THE CIMARRON RIVER [Source: Tyagi, 1988, p.4]

Overflow Structure	Maximum Scour Depth Location	Scour (feet)
1	Upstream	10.2
2	Downstream	27.0
3	Upstream	22.7
4	Downstream	12.2
5	Upstream	15.4
6	Downstream	11.4
7	Upstream	30.0
8	Downstream	10.7

The data contained in Tyagi's (1988) study were collected using an Electronic Distance Meter and a small boat some time after the flood had receded. This analysis revealed that the maximum scour depth, some time after the flood had receded, ranged from 10 to 30 feet. As can be seen from Table VII most of the deep scour holes were located on the upstream side of the structures where velocities could be expected to be the highest.

Modeling

Modeling Strategy

Strongylis (1988) demonstrated that due to the complex nature of the flow at this site it is suited for a two dimensional flow analysis. Additionally, given the incorporation of scour calculation capabilities into two dimensional modeling software the same software used for a hydraulic analysis may also be used for a scour analysis. Therefore, in this instance a hydraulic analysis of this site was completed and the results from this study used to complete the scour analysis . To complete the hydraulic and scour analysis the following resources were utilized:

1. The Surface Water Modeling System, Version 4.0, (SMS) developed by the Engineering Computer Graphics Laboratory at Brigham Young University was utilized for processing the data used in the hydraulic study.
2. To complete the hydraulic analysis, the Finite Element Surface-Water Modeling System: Two-Dimensional Flow in a Horizontal Plane, Version 2 (FESWMS-2DH), developed by the U.S. Department of Transportation Federal Highway Administration was used.
3. Additional information concerning procedure for conducting the scour analysis was gained from the U.S. Department of Transportation Federal Highway Administration's publication *HEC-18, Evaluating Scour at Bridges, Second Edition.*

Hydraulic Modeling

As mentioned previously the first step in constructing any hydraulic model consists of collecting all appropriate data. The data which was collected for use in modeling this site includes:

1. A 3.5 foot by 3.5 foot aerial photo (scale 1:200) of the site taken from an altitude of 2900 feet on 6-30-90.
2. Aerial photos (scale 1:200) of the site taken on 11-11-86 showing the scour damage done to the overflow bridges.
3. A contour map of the site made by G.F.M. & Associates.
4. O.D.O.T. construction plans dated from 1957 for the previously existing bridges.
5. O.D.O.T. study files and photographs.
6. The S.C.S. Soil Survey *Soil Survey of Payne County Oklahoma.*
7. Tyagi's 1988 Report No. 88-1 *Scour Around Bridge Piers of Overflow Structures at I-35 Bridge on the Cimarron River.*
8. Strongylis' 1988 report "*Water Surface Profiles Using FESWMS-2DH Model.*"

The information from items 1, 2, 3, 4 and 8, was used to design a finite element network representing the site. Information from items 3 and 4 was used to construct a contour map, for use in determining elevations, accurately representing the site prior to the 1986 flood. Items 1, 2 and 8 were used to determine roughness values for the element network. The resulting element network is included in Figure 14, Site Element Network.

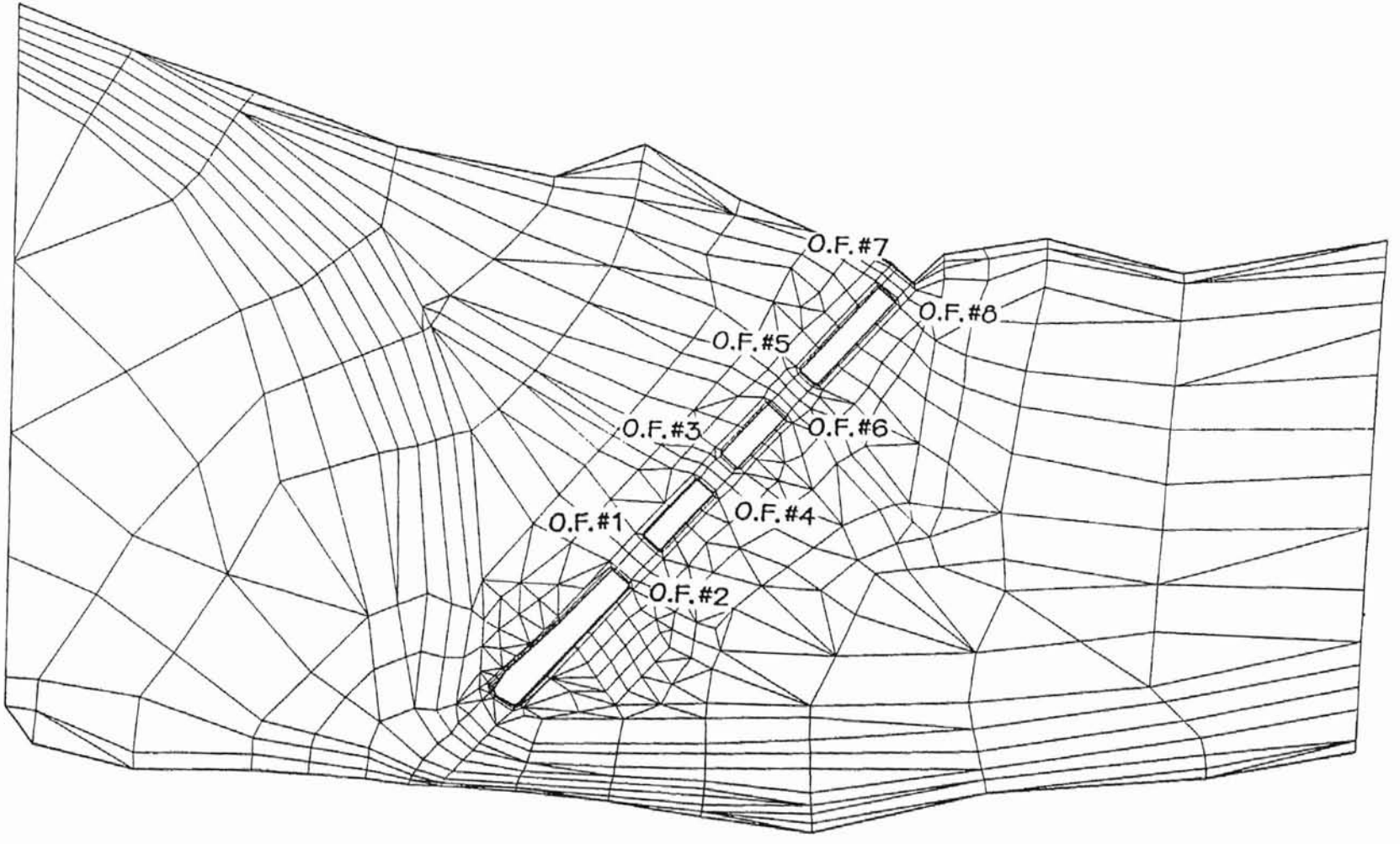

Figure 14. Site Element Network

Information describing the site was first entered in a "DINMOD" file of FESWMS-2DH Version 2.0. This information was then refined and corrected using the SMS computer software. SMS is a pre- and post-processor for two dimensional finite element and finite difference models. The SMS computer software greatly simplifies the inputting of a large amount of data and aids in checking it, by allowing these activities to be done in a graphic manner. SMS also provides the ability to check a finite element network to ensure the "correctness" of the network. This is done by locating elements with large aspect ratios, adverse grades, gaps in the finite element network, or other geometry type problems. Additionally, the "user friendly" environment allows a visual overview of the finite element network to ensure that the network constructed accurately represents the area being modeled.

For this application a mixture of six-node triangular, and nine-node quadrilateral elements were used. The element size was varied depending upon the hydraulic significance and geometric complexity of the area. Therefore, smaller elements were used near bridges and larger elements in the flood plain. Both quadrilateral and triangular elements were constructed by having their longer side parallel to the smaller gradient.

Using the SMS software element resequencing was performed to obtain a direct solution of the equation which results from the application of the finite element method, resequencing was performed in both the forward and backward direction, in relation to the site, using a variety of means. The smallest front width was obtained by using the minimum front-growth method in a backwards direction.

Often times use of the FESWMS-2DH software and "FLOMOD" module requires the use of a "cold start," "hot start" procedure. However, when modeling the

October 1986 flood with this model convergence of the residual equations could be obtained in one run. Completing the model in one run required the use of 15 iterations.

Once the finite element network was completed it was possible to calibrate the model to ensure the validity of the results. Some critical aspects of a finite element network include shape, size and placement of the elements, selection of manning n values, and selection of the kinematic viscosity. As mentioned previously, information from O.D.O.T.'s files showed that the October 1986 flood had a flow rate of 156,000 cubic feet per second and a downstream water surface elevation of 898.0 feet. The upstream flow rate of 156,000 cubic feet per second was used as an upstream boundary condition and the downstream water surface of 898.0 feet was used as a downstream boundary condition. The finite element network was changed and refined until the model yielded results which agreed with the available data which showed a lack of pressure flow at the bridges.

Several finite element networks were constructed, progressively refining the area of the overflow bridges, until a result was obtained from the FESWMS-2DH. Difficulty was found in modeling the high banks of the floodplain. As FESWMS-2DH tried to arrive at a solution these elements were successfully "wetted" and "dried" leading to instability in the solution. This problem was solved by eliminating all of the unnecessary "dry" elements from the network.

Mannings n values were chosen for the floodplain and channel areas according to standard engineering practice and text. These values were then varied, especially in the floodplain area, by up to 50%. This variance proved to have a small effect upon the FESWMS-2DH output, therefore, the n values originally assumed were used.

Kinematic eddy viscosity was varied from 10 to 100. A larger value, such as 100, helps lend numerical stability to the model, whereas, a smaller value, such as 10, is likely to be more accurate. A value of 10 was used for the kinematic eddy viscosity and this lead to numerical instability in the model. A high value of kinematic eddy viscosity resulted in an unrealistically high water surface. Therefore, a value of 15 was used to model the kinematic eddy viscosity.

Finally, after an accurate network had been built and calibrated it was used to model the flood in question and obtain scour results. As mentioned previously, the flood being studied had a flow rate of 156,000 cubic feet per second and a downstream water surface of 898.0 feet. Analysis and presentation of the output was also greatly simplified by use of the SMS computer software. A summary of the velocities resulting from the October 1986 flood are contained in Figure 15, Velocity Vectors for October 1986 Flood.

An upstream water surface of 901.8 feet was determined to correspond with a downstream water surface of 898.0 feet. This yields a water surface slope of 0.00036 feet per feet, while the flow line slope is 0.00045 feet per feet. The water surface slope is shallower than the flow line slope because the bridges tend to back up the water and flatten the water surface slope.

Scour Modeling

Using Version 2.0 of FESWMS-2DH allows scour calculations to be completed along with a hydraulic analysis. Clear-water contraction scour may be completed using a version of Laursen's clear-water scour equation given in Chapter 3. Pier scour may be completed by using either the Colorado State University equation, given in Chapter 3, or

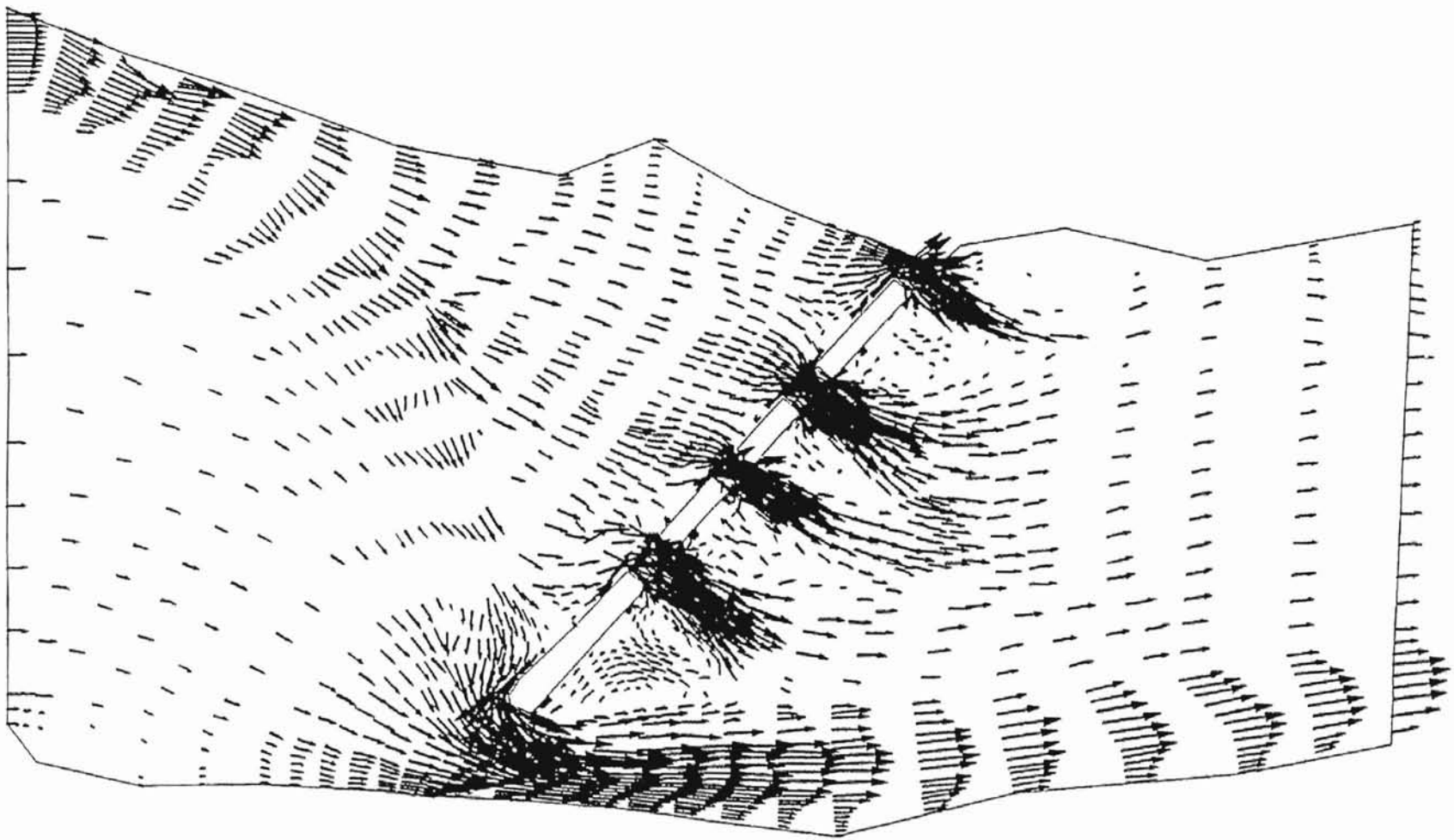

Figure 15. Velocity Vectors for October 1986 Flood

Froehlich's pier scour equation. A summary and analysis of the calculated scour results are given in the next chapter. A complete listing of the calculated scour data for each pier is included in Appendix E.

In this instance the values of velocity upstream of the overflow bridges were larger than the critical velocity. This condition would normally indicate that clear-water scour was occurring at the overflow bridges. However, in this case, as with many bridges on floodplains, the assumption of clear water scour was maintained. The assumption was maintained because:

1. There is vegetation growing on the floodplain.
2. The velocities are large enough that the fine bed material would probably go into suspension at the bridge and not influence the contraction scour.

Computation of contraction scour was accomplished by inputting the correct n value information and the critical shear value, τ_c, for the elements where contraction scour was to be modeled. This consisted of all elements in the vicinity of the overflow bridges. According to the recommendations in HEC-18 the shear value was chosen based upon the value of $1.25(D_{50})$. Again, this procedure was greatly simplified and verified by using the SMS computer software .

Pier data was entered in SMS not only for the scour modeling but to improve the accuracy of the hydraulic modeling. In this instance the Colorado State University Equation was used to predict pier scour. According to the methods outlined in HEC-18 the five piles in the pile bent were entered as one pier having a width of 6.66 feet. Additionally, according to HEC-18 since the Froude numbers at the bridge sites were less than 0.8 the value of y_s/a was limited to 2.4, or to a maximum scour depth of 3.2 feet.

CHAPTER V

RESULTS AND DISCUSSION

Summary of Results

Calculated scour amounts for all of the overflow bridges are given in Table VIII, Comparison of Actual to Calculated Scour. Table VIII lists not only the actual scour recorded at each bridge but also the scour calculated at each bridge. The calculated scour given in Table VIII represents the calculated contraction scour only. Scour values given in Table VIII do not account for the depth, or width, of piers, which limit pier scour, or the presence of "Red Bed" which may have also limited the contraction scour.

TABLE VIII

COMPARISON OF ACTUAL TO CALCULATED SCOUR

Overflow Structure	Recorded Scour (Tyagi, 1988) (Feet)	Calculated Contraction Scour (Feet)
1	10.2	33.3
2	27.0	29.6
3	22.7	32.9
4	12.2	28.6
5	15.4	26.6
6	11.4	28.6
7	30.0	27.2
8	10.7	28.2

As can be seen from Table VIII the maximum scour at all of the overflow bridges except numbers 1 and 2 occurred at the upstream bridges, the odd numbered bridges. At bridges 1 and 2 the maximum scour occurred at the downstream bridge, number 2. Inspection of Figure 15, Velocity Vectors for October 1986 Flood, given previously, shows that the velocity vectors upstream of bridges 1 and 2 appear more jumbled and less streamlined than those upstream of the other overflow bridges. Therefore, the large scour probably did not occur upstream of bridges 1 and 2 because the flow was less defined in this area when compared to the other bridges.

Figures 16, 17, 18, and 19 compare the actual scour to the calculated scour at the upstream faces of overflow bridges 1, 3, 5, and 7, respectively. The deepest actual scour along with the scour occurring at these locations is shown in these figures. Similar figures were not included for overflow bridges 2, 4, 6 and 8, the downstream bridges, because by the time the actual sour was recorded fill had been placed around these bridges to add support to their piers. Figures 16, 17, 18 and 19 show a breakdown of the calculated contraction and pier scour and limit the pier scour to $2.4(y_s/a)$.

The actual scour occurred over a large area, as shown in Appendix D, not just under the bridges. However calculated contraction and pier scour can only be applied at the bridge sections or piers. Additionally, when calculating contraction and pier scour obtaining the actual limits which occurred in this case would be difficult. The reason why scour occurred over this large area is unknown but probably has to do with the increased velocities resulting from the bridges at these points.

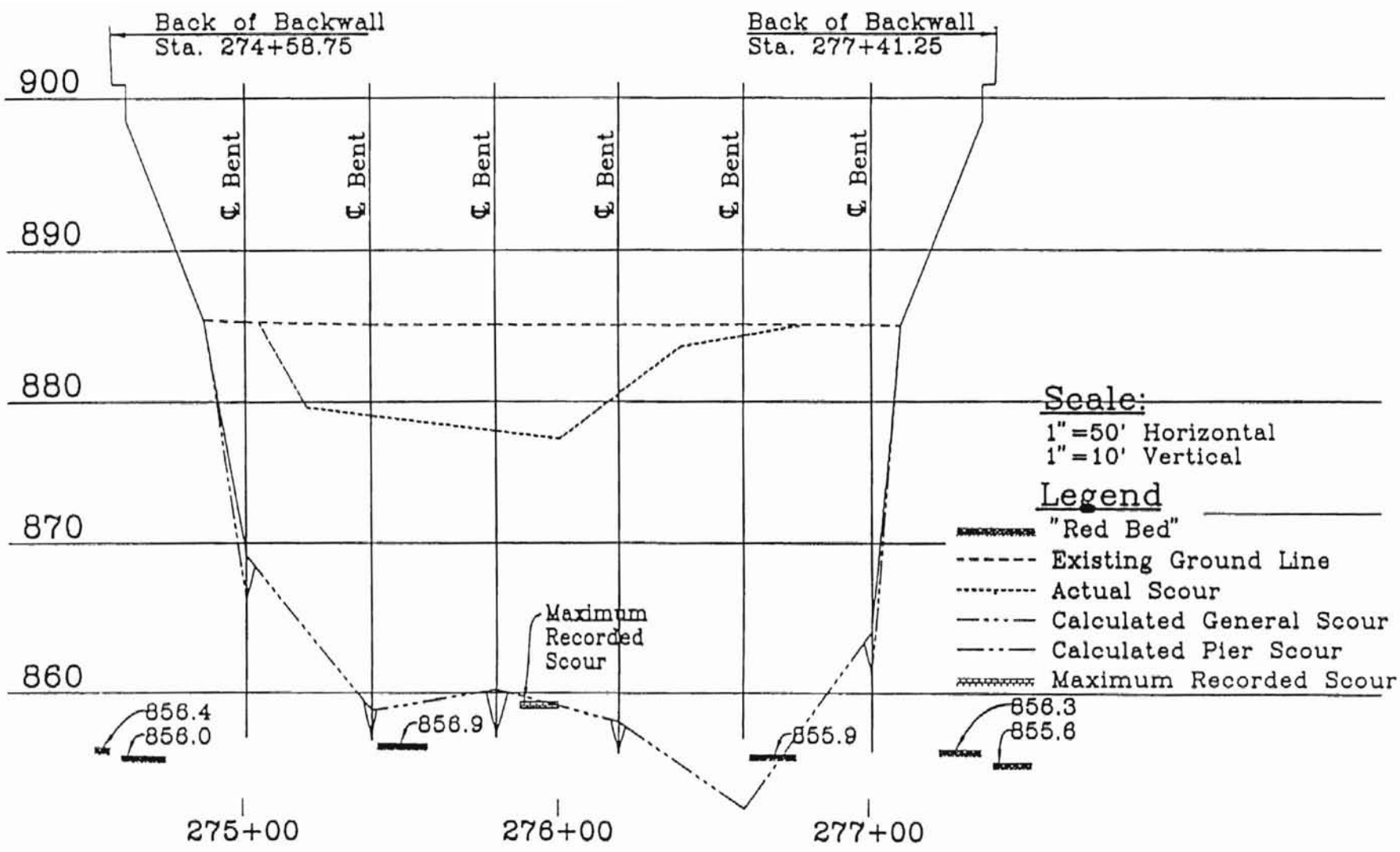

Figure 16. Calculated Versus Actual Scour Upstream of Overflow Bridge 1

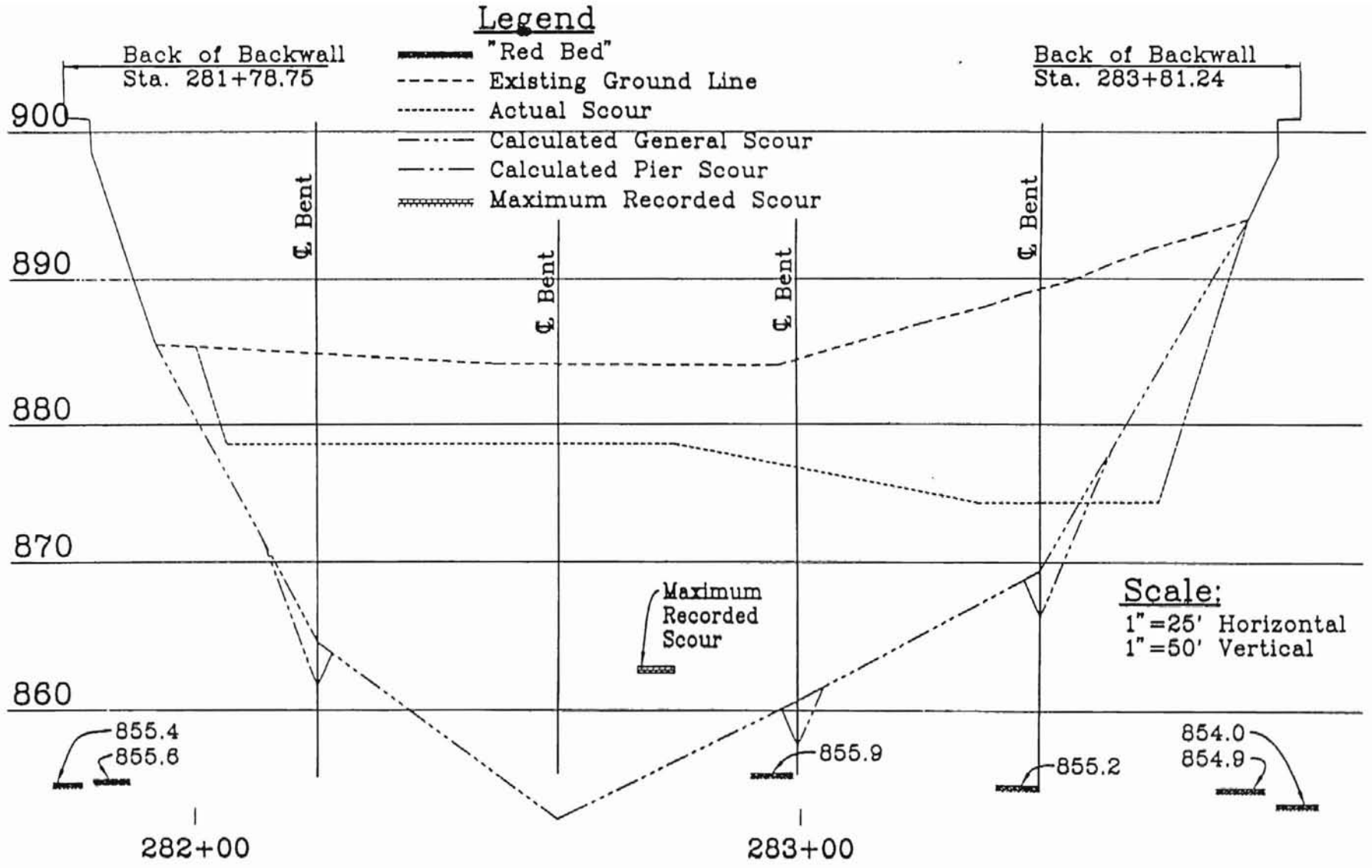

Figure 17. Calculated Versus Actual Scour Upstream of Overflow Bridge 3

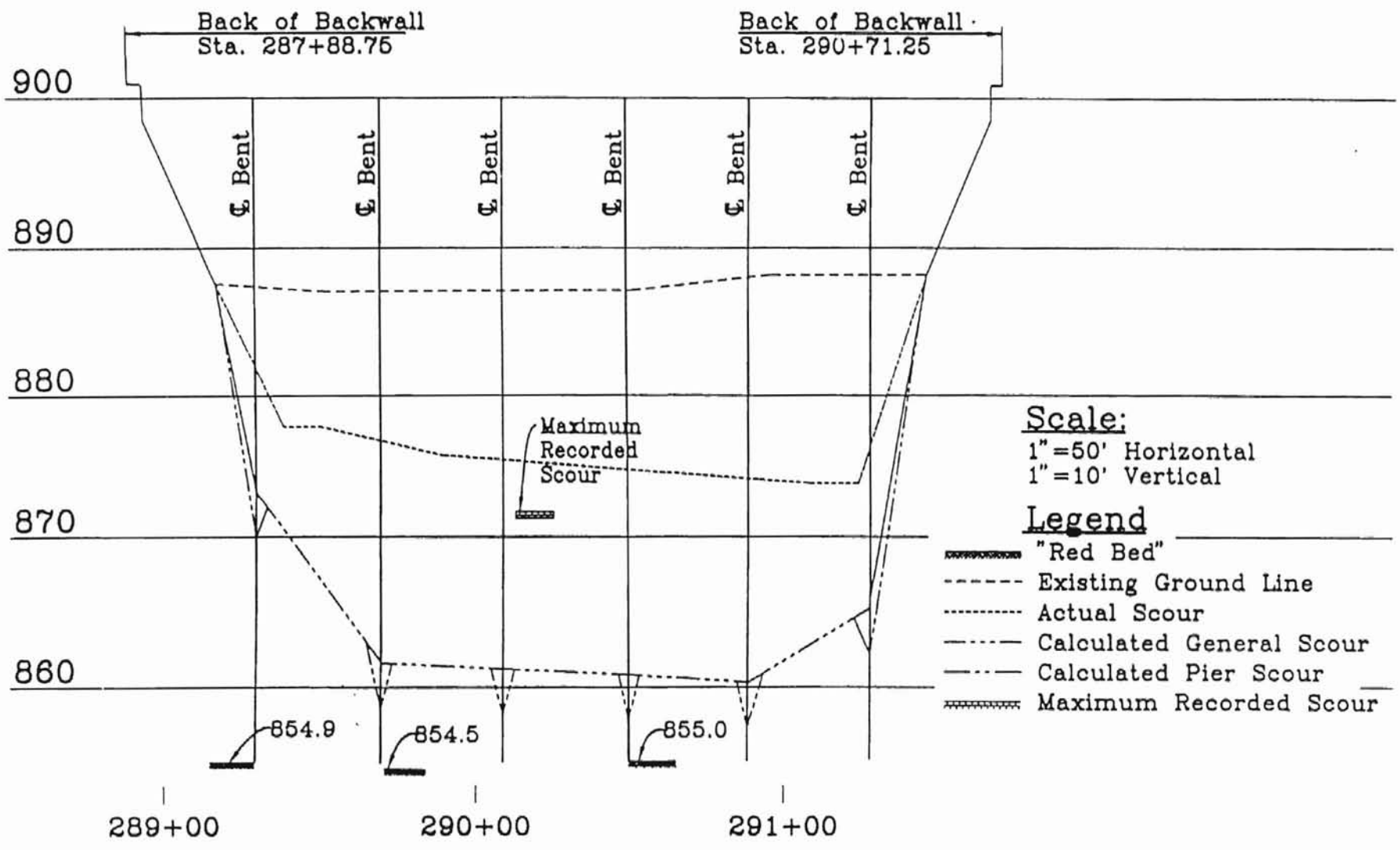

Figure 18. Calculated Versus Actual Scour Upstream of Overflow Bridge 5

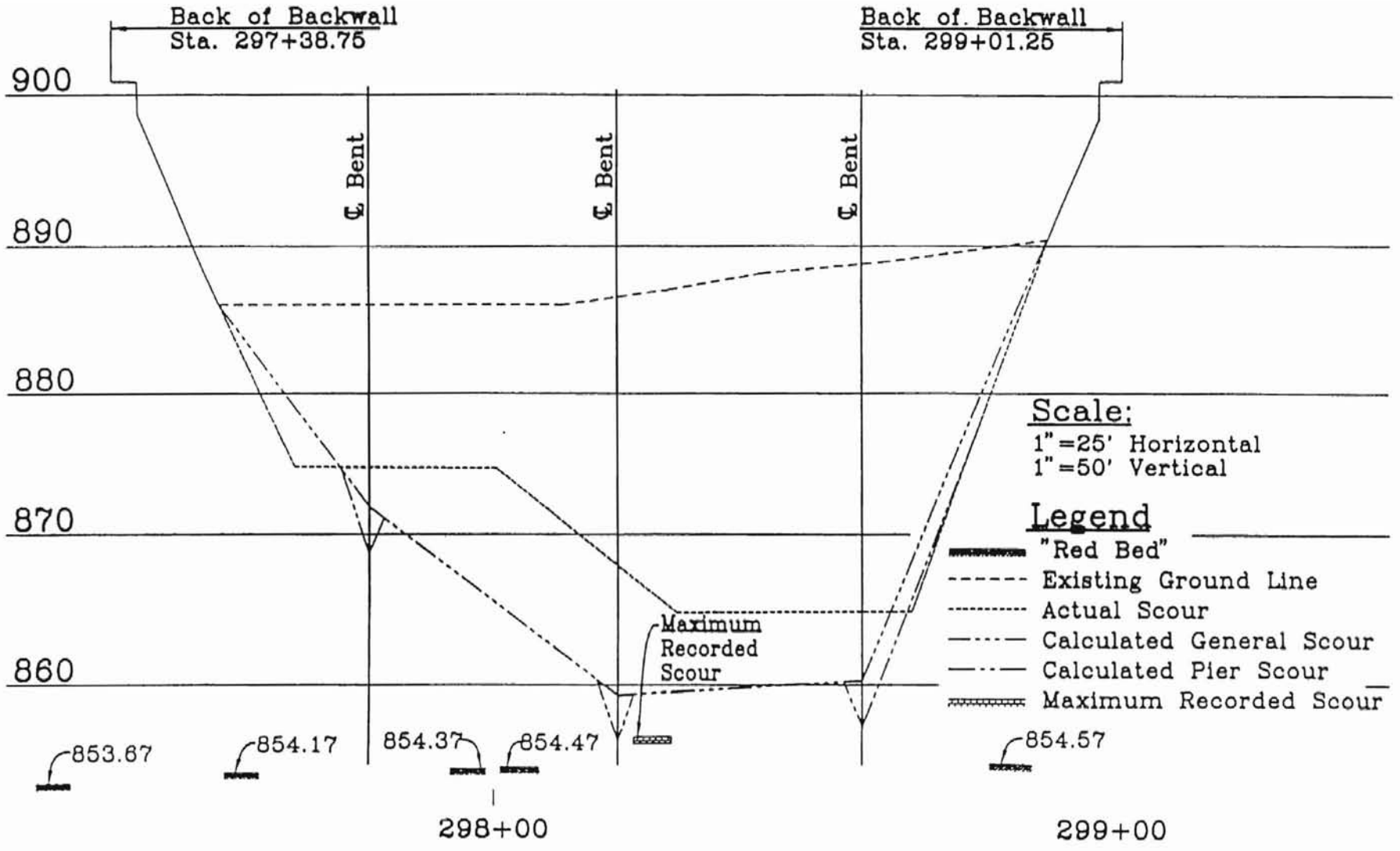

Figure 19. Calculated Versus Actual Scour Upstream of Overflow Bridge 7

Discussion of Results

As can be seen from Table VIII the calculated contraction scour ranged from 26.6 feet to 33.3 feet, whereas, the recorded scour ranged from 10.2 feet to 30.0 feet. The largest actual scour of 30.0 feet corresponded to a calculated contraction scour of 27.2 feet. The smallest actual scour of 10.2 feet corresponded to a calculated scour of 33.2 feet, the largest calculated contraction scour.

As can be seen from Figures 16 to 19 no difference between contraction and pier scour was apparent in the recorded scour. Pier scour may have occurred only not to be recorded because it was obscured during measurement of the scour by water in the holes. Additionally, review of Table VIII and Figures 16 to 19 reveals that the "Red Bed" layer may have limited the actual scour which occurred.

In all instances, except at overflow structure number 7, the calculated contraction scour was larger than the recorded scour. The maximum calculated scour, since it was calculated using the clear-water scour and Colorado State University pier scour equations, varied little from bridge to bridge since the maximum velocities and water depths were similar at each bridge. However, actual scour varied from bridge to bridge with maximum scour values generally being upstream of the bridges.

It should also be noted that the scour equations, mentioned above, are generally used to yield a "design" value and not a maximum predicted value. Therefore, a comparison of calculated to actual scour should yield a calculated scour near to or greater than the actual scour.

As mentioned above the calculated contraction scour is generally larger that the actual scour. These differences may be due to the following reasons:

1. The actual scour was recorded some time after the actual flood had occurred, therefore, some filling of the scour holes should have occurred during the receding portion of the food.
2. From reviewing the aerial photos it appears that there may have been significant movement of soil particles into and out of the scour holes, therefore, the scour may have been clear-water scour and not live-bed scour. However, for the reasons mentioned previously, this is unlikely.
3. The actual scour may have been limited in depth by the "Red Bed" layer.
4. The scour equations tend to over predict scour and are intended for use as a design tool and not to predict actual scour depths.

CHAPTER VI

CONCLUSIONS AND RECOMMENDATIONS

Conclusions

Based upon the results of this study the following conclusions may be made:

1. Microcomputer applications of the FESWMS-2DH computer program may be used to successfully perform the hydraulic analysis of complex river crossings such as the Cimarron River and Interstate-35. FESWMS-2DH reports depth averaged point velocities, direction and point water surface elevations . FESWMS-2DH is a powerful two dimensional surface water flow analysis program which may correctly analyze complex flow problems much more readily than traditional one dimensional methods.
2. The SMS computer program greatly enhances the pre- and post-processing of the data used in a two dimensional flow analysis. The SMS computer program also aids on checking the validity of a model by providing "user friendly" viewing, checking and updating of that model. In short the SMS computer program is a powerful graphical users interface for use by engineers performing two dimensional surface water flow analysis.
3. The results from the hydraulic analysis performed in this study appear reasonable and correct. The calculated water surface values provide close agreement with information contained in O.D.O.T.'s files. O.D.O.T. files

described a flow rate of 156.000 cubic feet per second, a downstream water surface elevation of 898.0 feet and a lack of pressure flow at the bridges.

4. The scour values calculated in this study are generally larger than the maximum recorded scour values. Some of this over prediction is expected, and help ensure a valid design tool. Several reasons may have contributed to this over prediction and these are outlined in the previous chapter.

5. The scour equations provide values useful in design but not necessarily useful in the prediction of actual scour values. Had an analysis of this type been performed as a portion of the design of the previously existing bridges, the flaws in their design and their susceptibility to scour type problems would have been apparent.

Recommendations

Based upon the results of this study the following recommendations may be made:

1. The scour equations outlined in *HEC-18 Evaluating Scour at Bridges,* and contained in the FESWMS-2DH computer program, tend to over predict actual scour values. These equations are based upon theoretical assumptions and laboratory data. Little attempt to calibrate these equations to actual field data has been made. More work needs to be performed to correlate the scour equations to actual scour data.

2. Although the scour equations tend to be conservative, the combination of scour analysis techniques and two dimensional flow analysis provides the engineer with a useful and powerful tool for predicting scour, and analyzing complex river crossings.

REFERENCES

Becker, L.D. (1994). Investigation of bridge scour at selected sites on Missouri streams. Water-resources investigations report 94-4200. Denver, CO: U.S. Geological Survey.

Chaudhry, M.F. (1993). Open-channel flow. Englewood Cliffs, NJ.: Prentice-Hall.

Chiew, Y. (1992). Scour protection at bridge piers. Journal of Hydraulic Engineering. American Society of Civil Engineers, Vol. 118, No. 9, 1260 - 1269.

Finnie, J.I., & Jeppson, R.W. (1991). Solving turbulent flows using finite elements. Journal of Hydraulic Engineering. American Society of Civil Engineers, Hydraulic Division, Vol. 117, No. 11, 1513 - 1530.

Froehlich, D.C. (1996). Finite element surface water modeling system: Two-dimensional flow in a horizontal plane, Version 2, Draft user's manual. McLean Virginia: Federal Highway Administration.

Froehlich, D.C. (1992). Finite element surface water modeling system: Two-dimensional flow in a horizontal plane, Version 2, User's manual preprint. McLean Virginia: Federal Highway Administration.

Gilbert, J.J., & Myers, D.R. (1989). Analysis of water surface and flow distribution for the design flood at a proposed highway crossing at the Sabine River near Tatum, Texas. Water-resources investigations report 88-4231. Denver, CO: U.S. Geological Survey.

Hydrologic Engineering Center. (1993). HEC-6 scour and deposition in rivers & reservoirs user's manual. Davis, CA: U.S. Army Corps of Engineers.

Lagasse, P.F., Schall, J.D., Johnson, F., Richardson, E.V., Richardson, J.R., & Chang, F. (1991). HEC-20 stream stability at highway structures. Washington, D.C.: Federal Highway Administration.

Laursen, E.M. (1960). Scour at bridge crossings. Journal of the Hydraulics Division. Proceedings of the American Society of Civil Engineers, Vol. 86, No. HY2, 39 - 54.

Laursen, E.M. (1963). An analysis of relief bridge scour. Journal of the Hydraulics Division. Proceedings of the American Society of Civil Engineers, Vol 89, No. HY3, 93 - 118.

Lee, J. K., & Froehlich, D.C. (1986). Review of literature on the finite element solution of the equations of two-dimensional surface water flow in the horizontal plane. U.S. Geological Survey circular 1009. Denver, CO.: U.S. Geological Survey.

Melville, B.W. and Dongol, D.M. (1992). Bridge pier scour with debris accumulation. Journal of Hydraulic Engineering. American Society of Civil Engineers, Hydraulic Division, Vol. 118, No. 9, 1306 - 1310.

Melville, B.W. (1992). Local scour at bridge abutments. Journal of Hydraulic Engineering. American Society of Civil Engineers, Hydraulic Division, Vol. 118, No. 4, 615 - 631.

Molinas, A. (1990). User's manual for BRISTARS (bridge steam tube model for alluvial river simulation). National Cooperative Highway Research Program, Project No. MR 15-11. Fort Collins, CO.: Hydrau-Tech, Inc..

Richardson, E.V., Harrison, C.J., Richardson, J.R., & Davis, S.R. (1993). HEC-18 evaluating scour at bridges, Second edition. Washington, D.C.: Federal Highway Administration.

Strongylis, D.G. (1988). Water surface profiles using FESWMS-2DH model. Norman, OK: The University of Oklahoma. (Unpublished master's thesis).

Tyagi, A.K. (1988). Scour around bridge piers of the overflow structures at I-35 bridge on the Cimarron River. Stillwater, OK: School of Civil Engineering, Oklahoma State University.

United States Geological Survey (1989). Soil survey of Payne County, Oklahoma. Washington D.C.: U.S. Department of the Interior.

Yalin, M.S. (1992). River mechanics. Oxford, England: Pergamon Press.

Zienkiewicz, O.C. (1977). The finite element method (3rd ed.). Maidenhead, England: Mc-Graw Hill.

APPENDIX A

SITE MAP

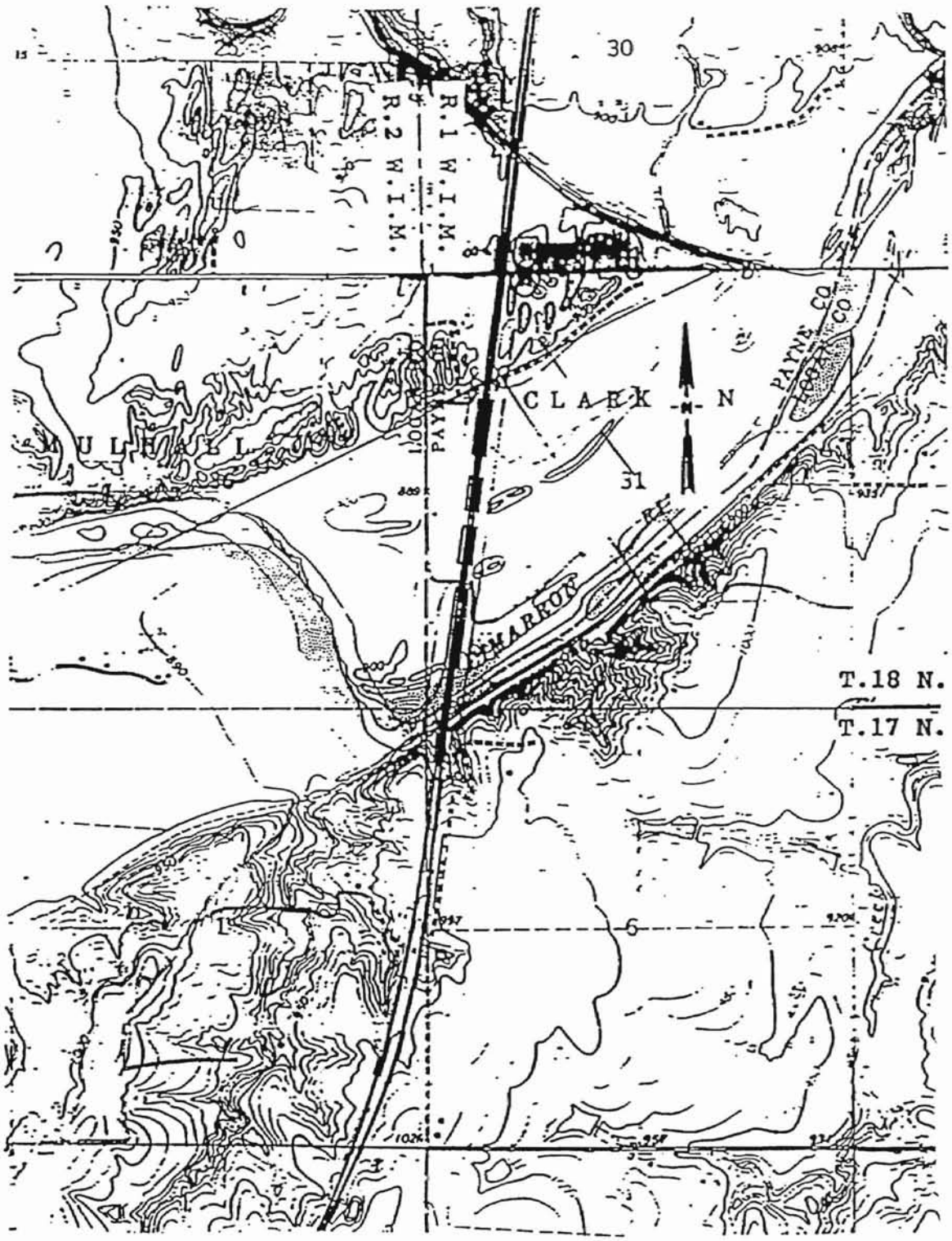

Site Map. Pre-1987 Conditions. Langston 7 1/2 min Quandrangle Map Photorevised 1983. Scale: 1"=2000 feet

APPENDIX B

HYDROLOGY DATA

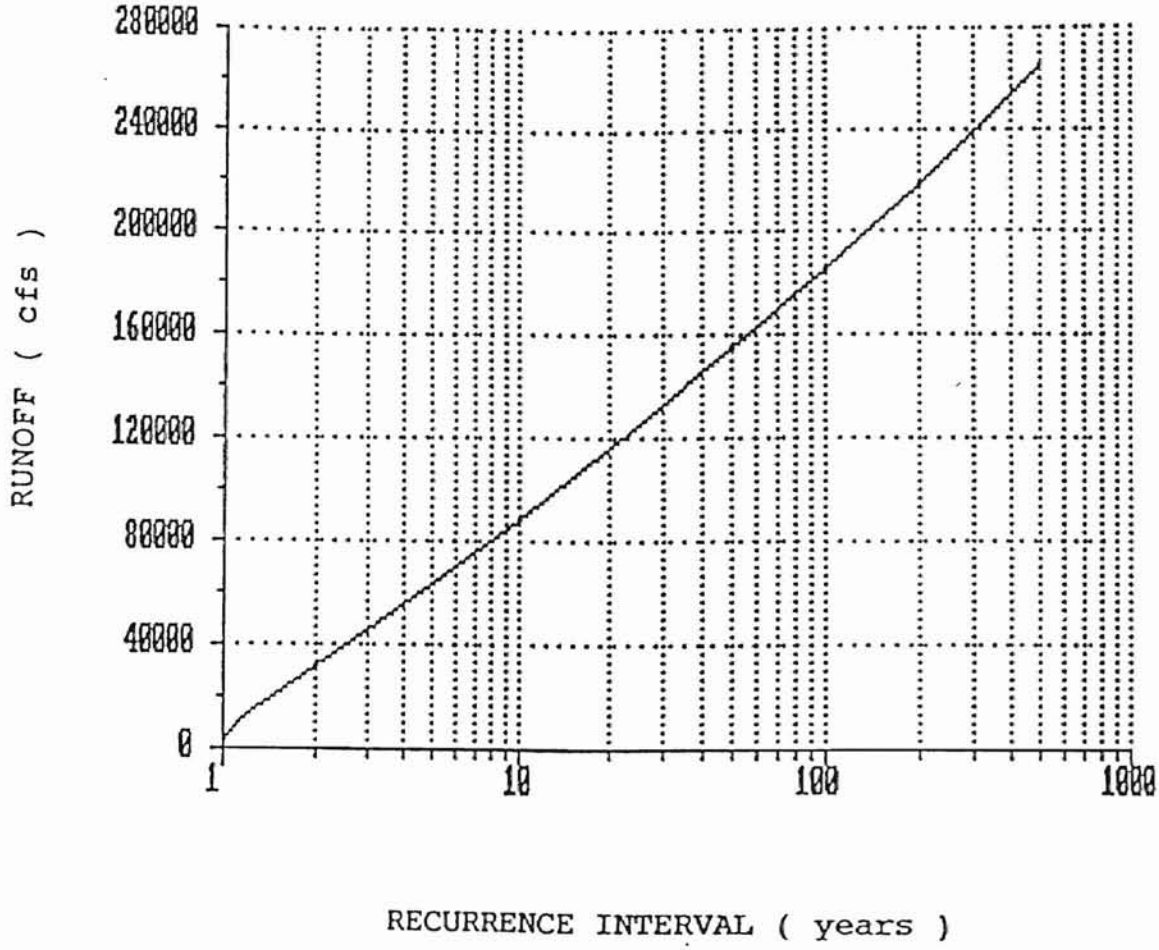

Runoff versus Recurrence Interval Curve

[Source: Strongylis (1992)]

APPENDIX C

SOILS DATA

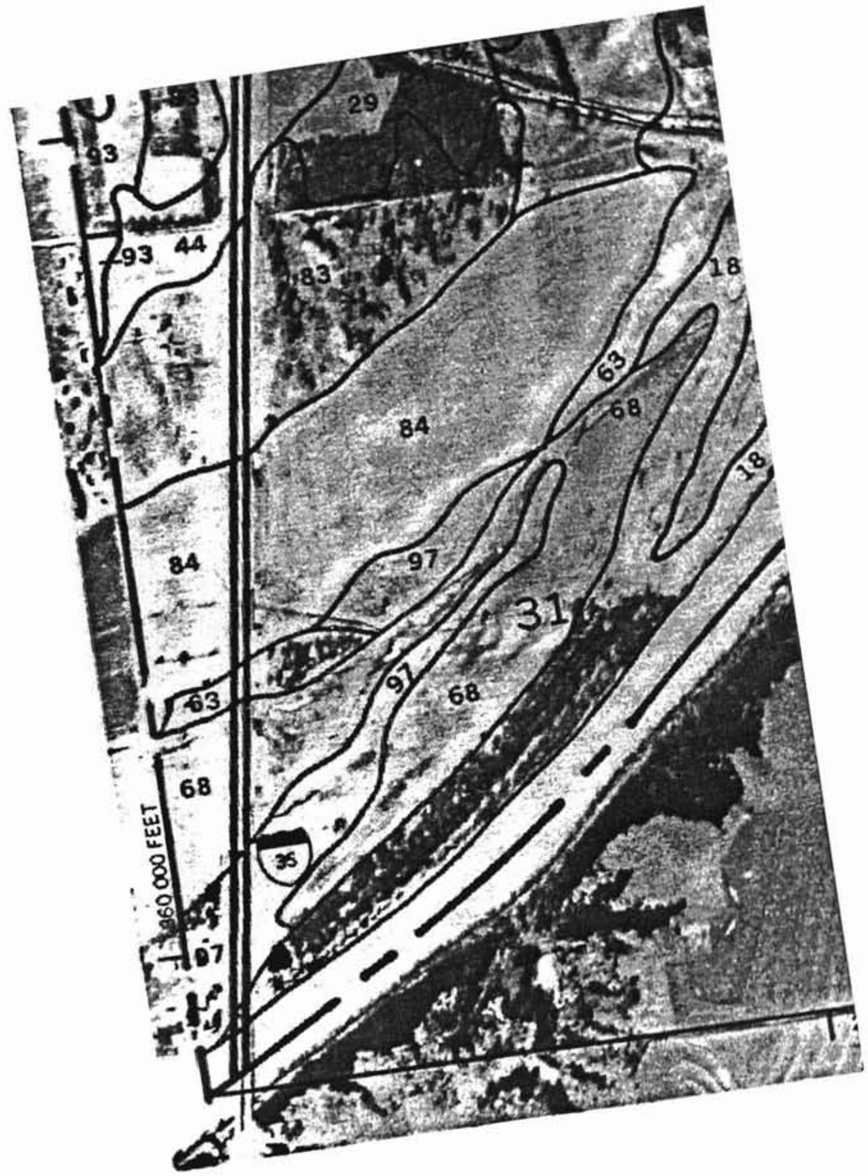

[Source: Soil Survey of Payne County, Oklahoma]

68---------- Yahola	0-8	Fine sandy loam	SM, ML, CL-ML, SM-SC	A-4	0	100	95-100	90-100	36-60	<26	NP-7
	8-46	Fine sandy loam, loam, very fine sandy loam.	SM, ML, CL SC	A-4	0	100	95-100	90-100	36-85	<30	NP-10
	46-64	Stratified loam to loamy fine sand.	SM, ML, CL SC	A-2, A-4	0	100	95-100	90-100	15-85	<30	NP-10
84---------- Hawley	0-10	Fine sandy loam	ML, SM	A-4	0	100	98-100	94-100	36-60	<26	NP-4
	10-32	Fine sandy loam, loam.	SM, SC, SM-SC, CL-ML	A-4	0	100	98-100	90-100	45-75	<30	NP-10
	32-60	Stratified loamy fine sand to silty clay loam.	SM, ML, SM-SC, CL-ML	A-2, A-4	0	100	98-100	90-100	30-70	<30	NP-7

APPENDIX D

SCOUR DATA

This appendix contains applicable portions of the report, *Scour Around Bridge Piers of Overflow Structures at I-35 Bridge on the Cimarron River*, by A.K. Tyagi (1988).

TABLE I

Maximum Scour Depths Near Structures C Through J at I-35 Bridge on the Cimarron River

Span Structure	Scourhole (feet)	Maximum Scour Depth Location	(feet)
P	281.33	Upstream	30.0
O	281.33	Downstream	10.7
N	201.33	Upstream	15.4
M	201.33	Downstream	11.4
L	281.33	Upstream	22.7
K	281.33	Downstream	12.2
C	161.33	Upstream	10.2
D	161.33	Downstream	27.0

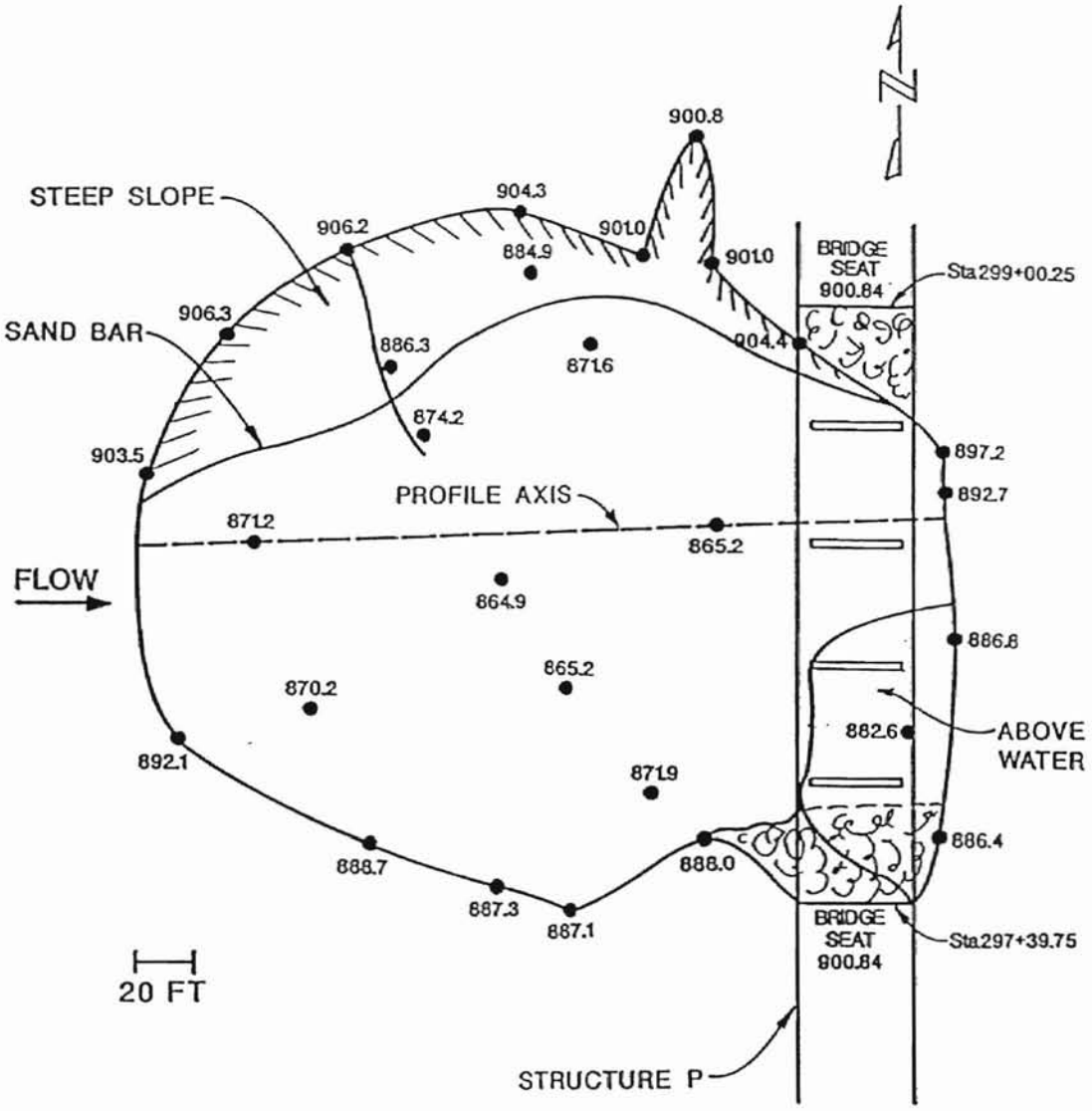

Figure 2. Location of Scour Hole Upstream of Structure P.

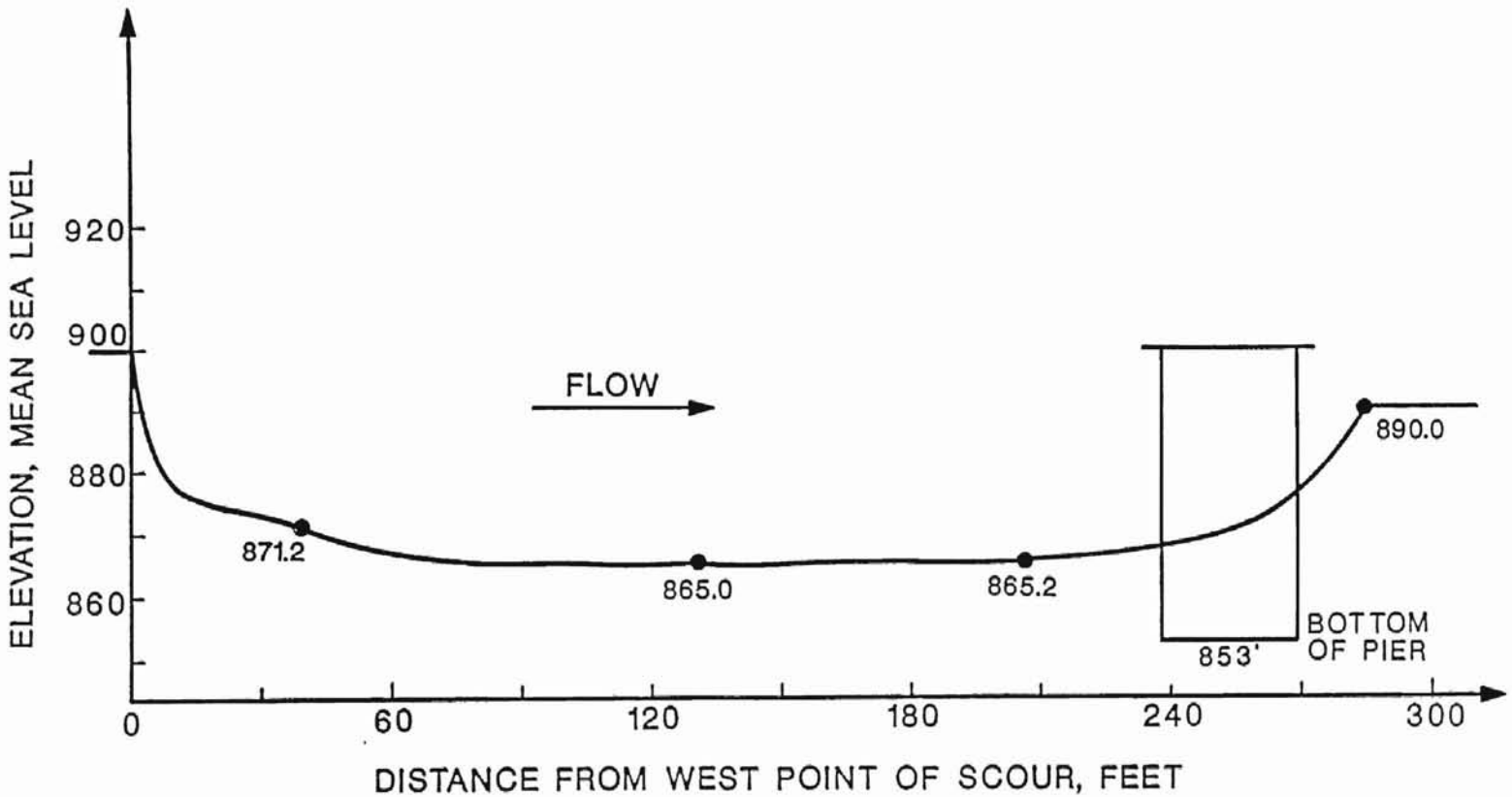

Figure 3. Profile of Scour Hole Upstream of Structure P.

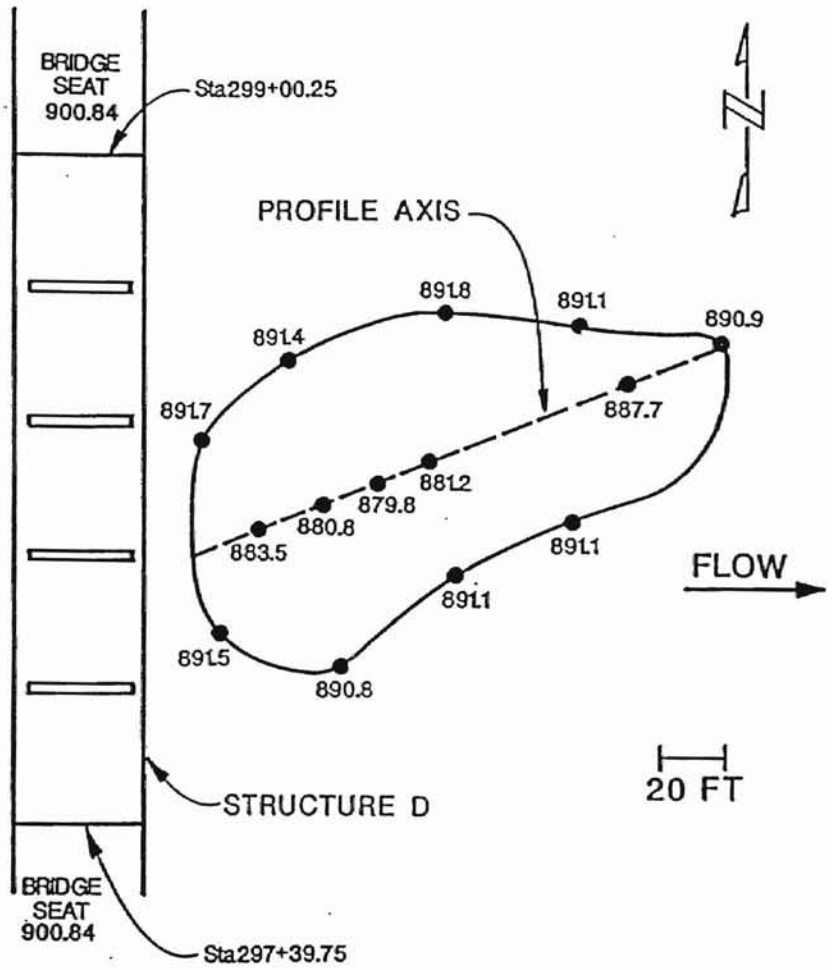

Figure 4. Location of Scour Hole Downstream of Structure O.

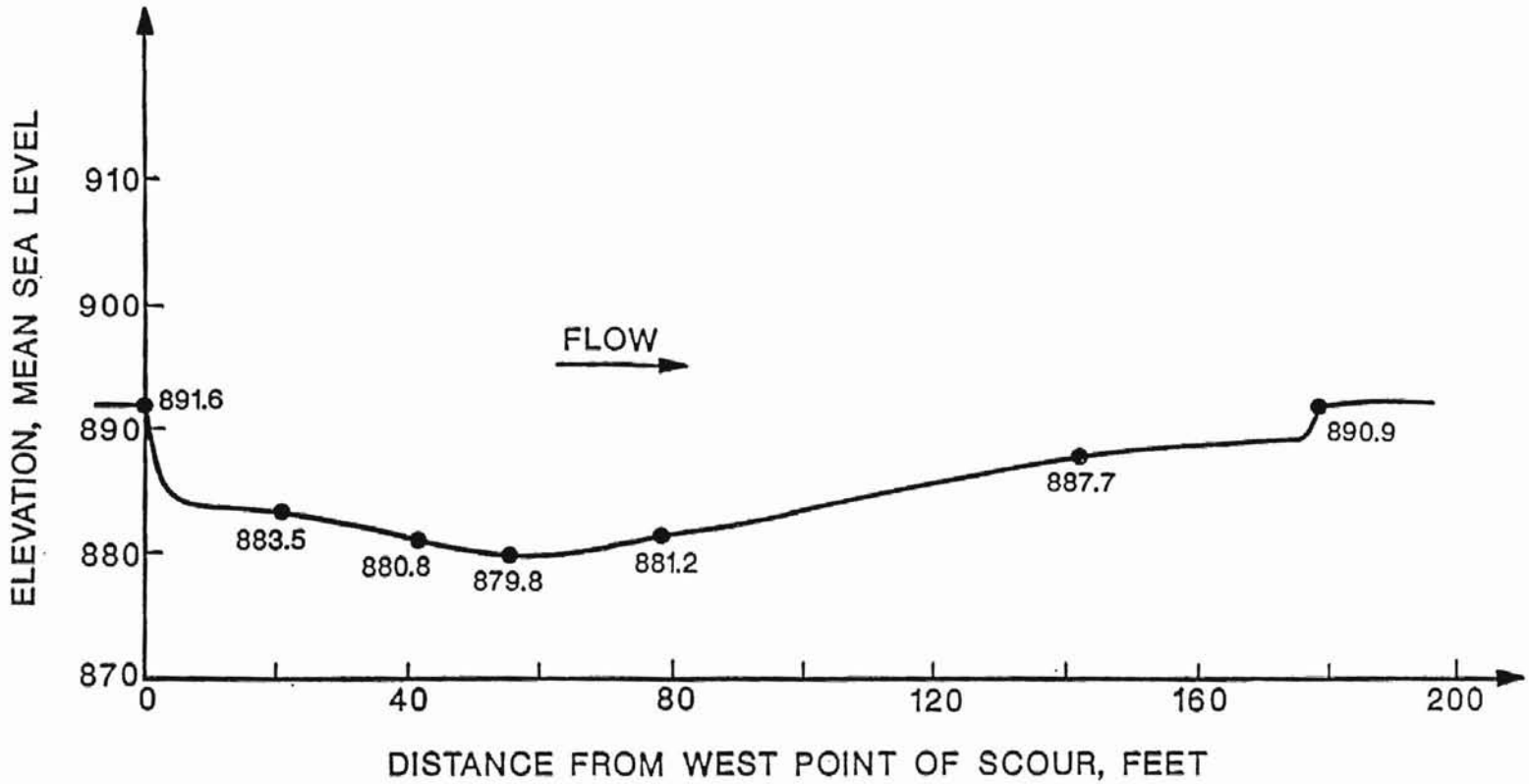

Figure 5. Profile of Scour Hole Downstream of Structure O.

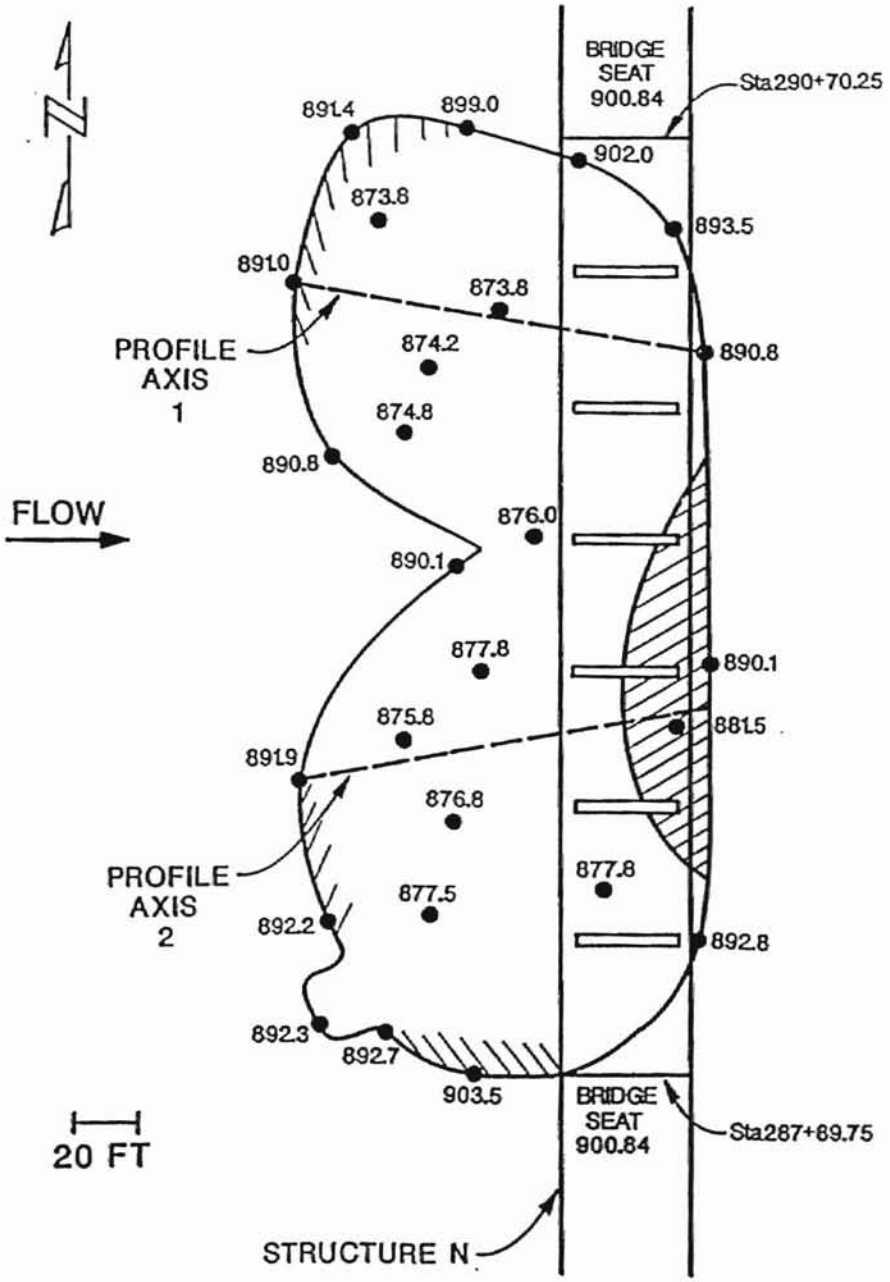

Figure 6. Location of Scour Hole Upstream of Structure N.

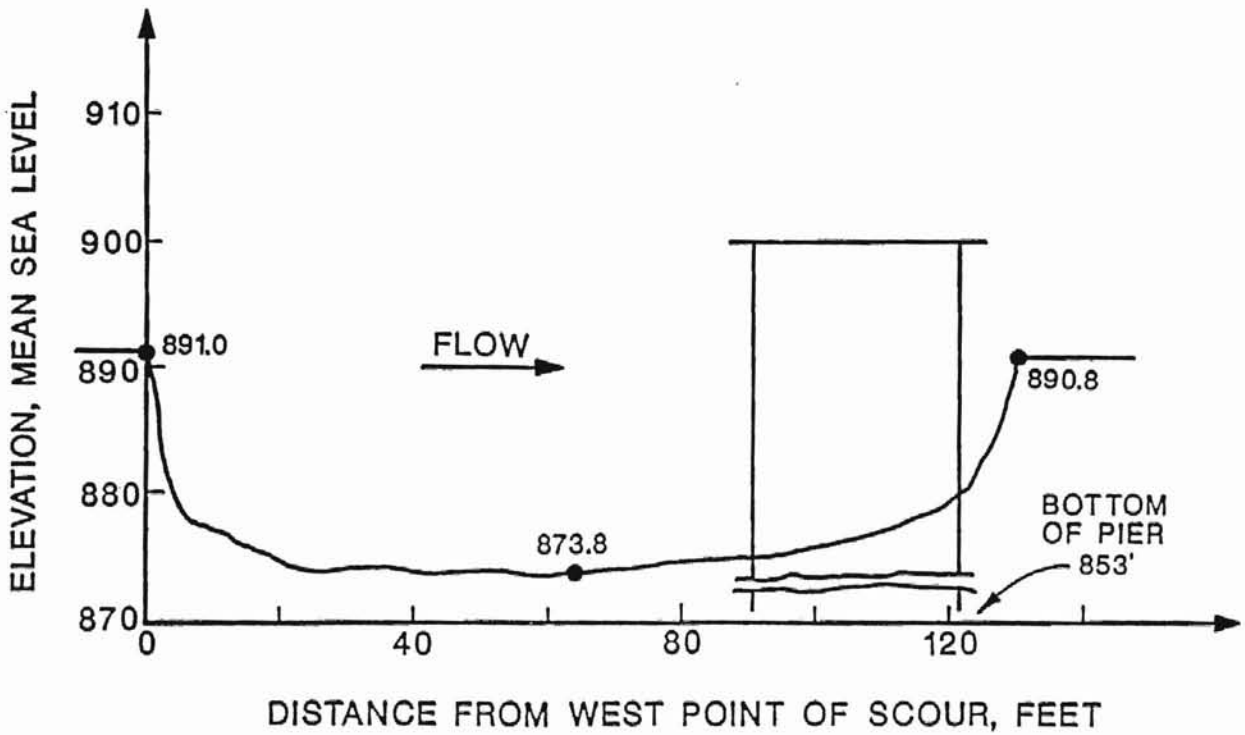

Figure 7a. Profile of North Scour Hole Upstream of Structure N.

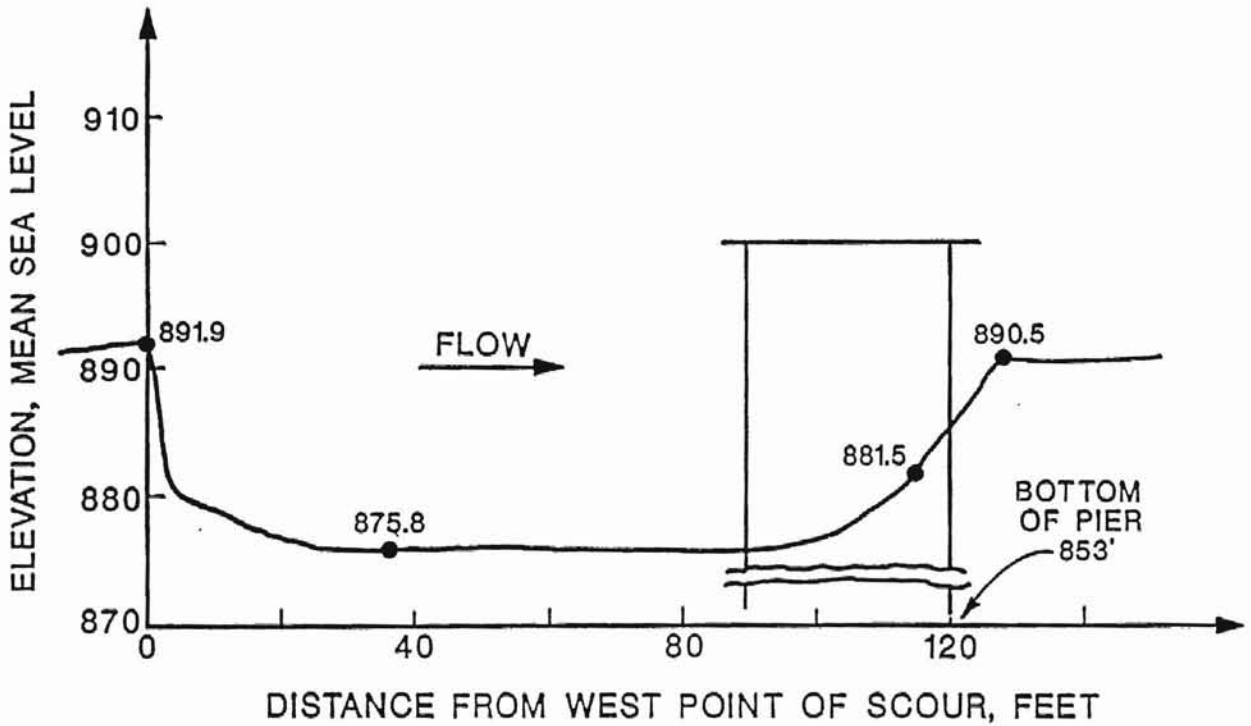

Figure 7b. Profile of South Scour Hole Upstream of Structure N.

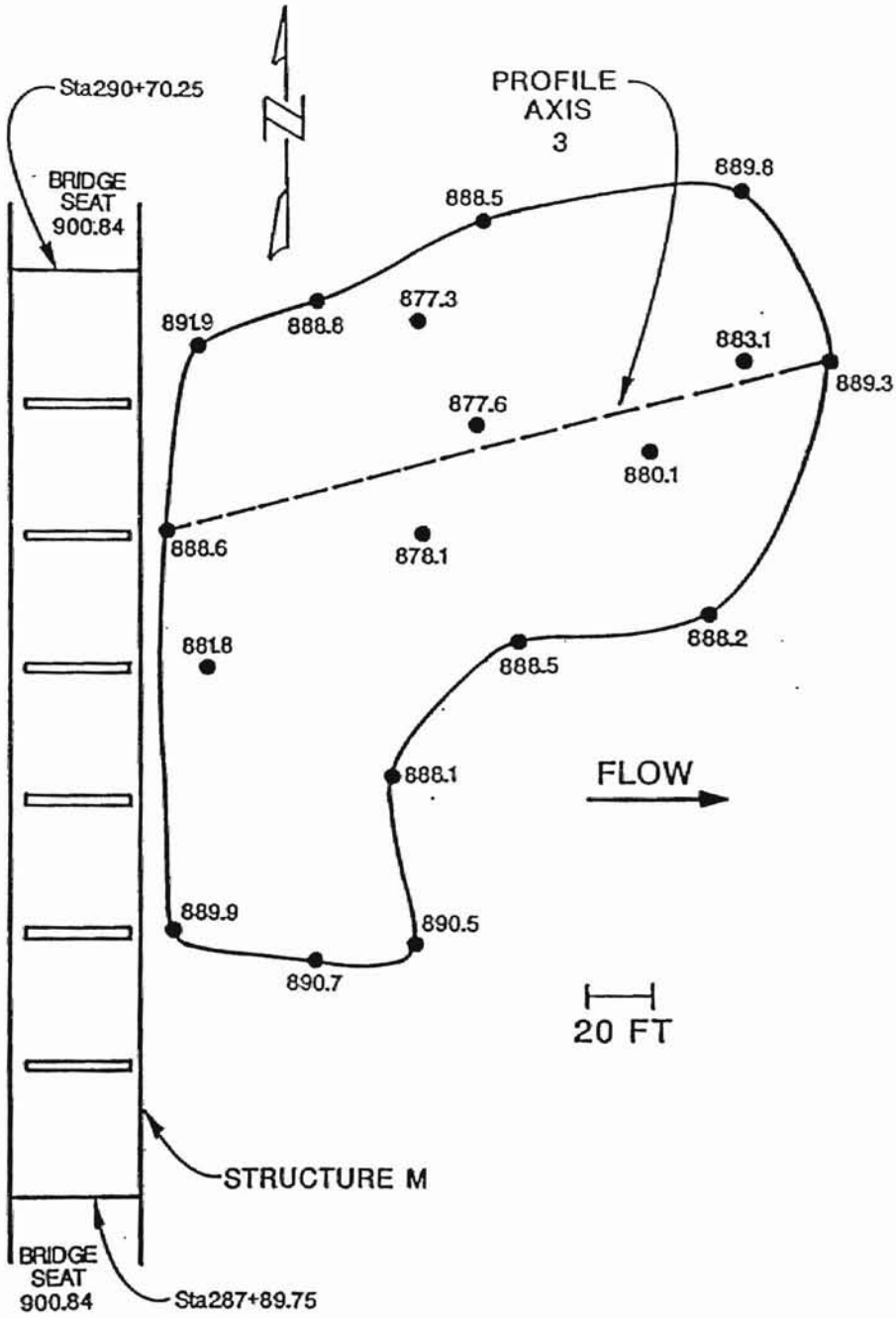

Figure 8. Location of Scour Hole Downstream of Structure M.

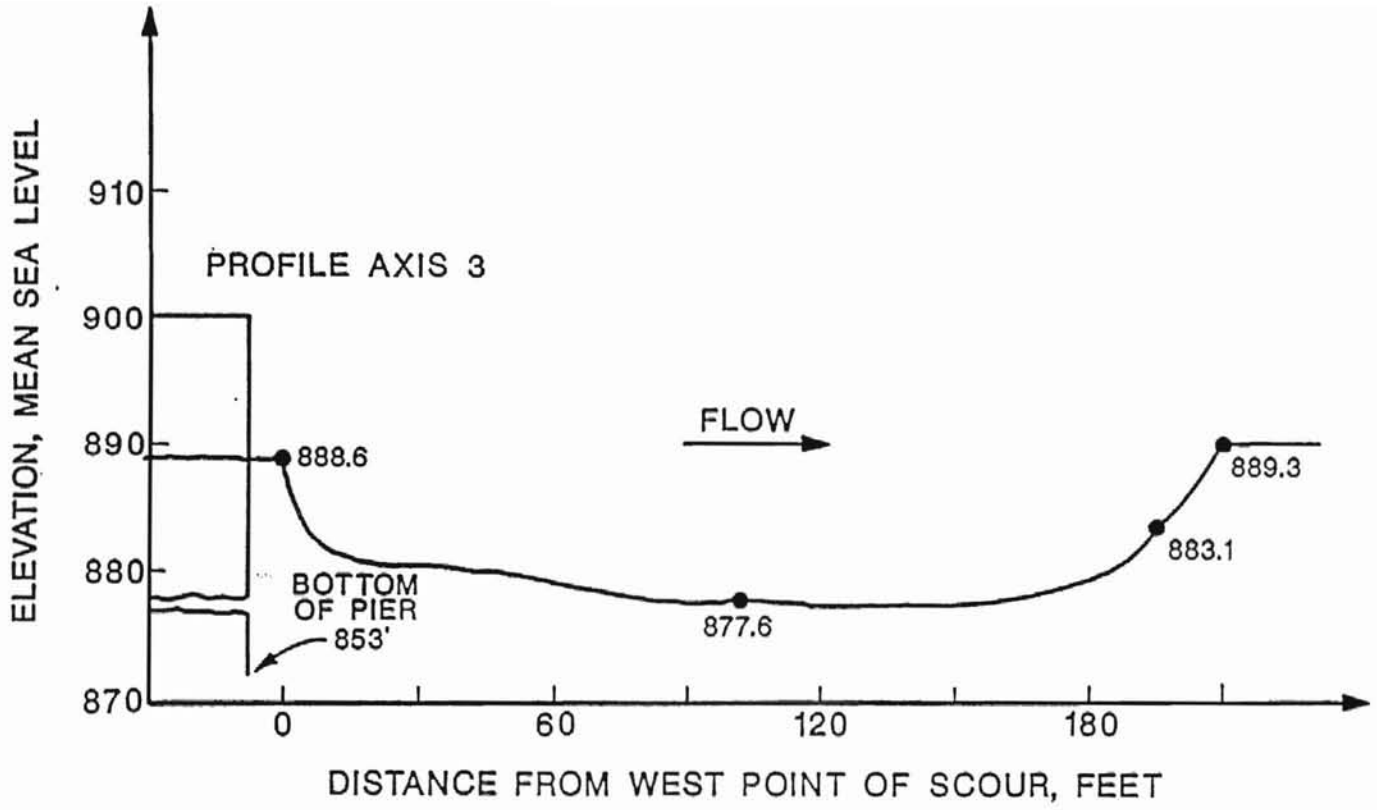

Figure 9. Profile of Scour Hole Downstream of Structure M.

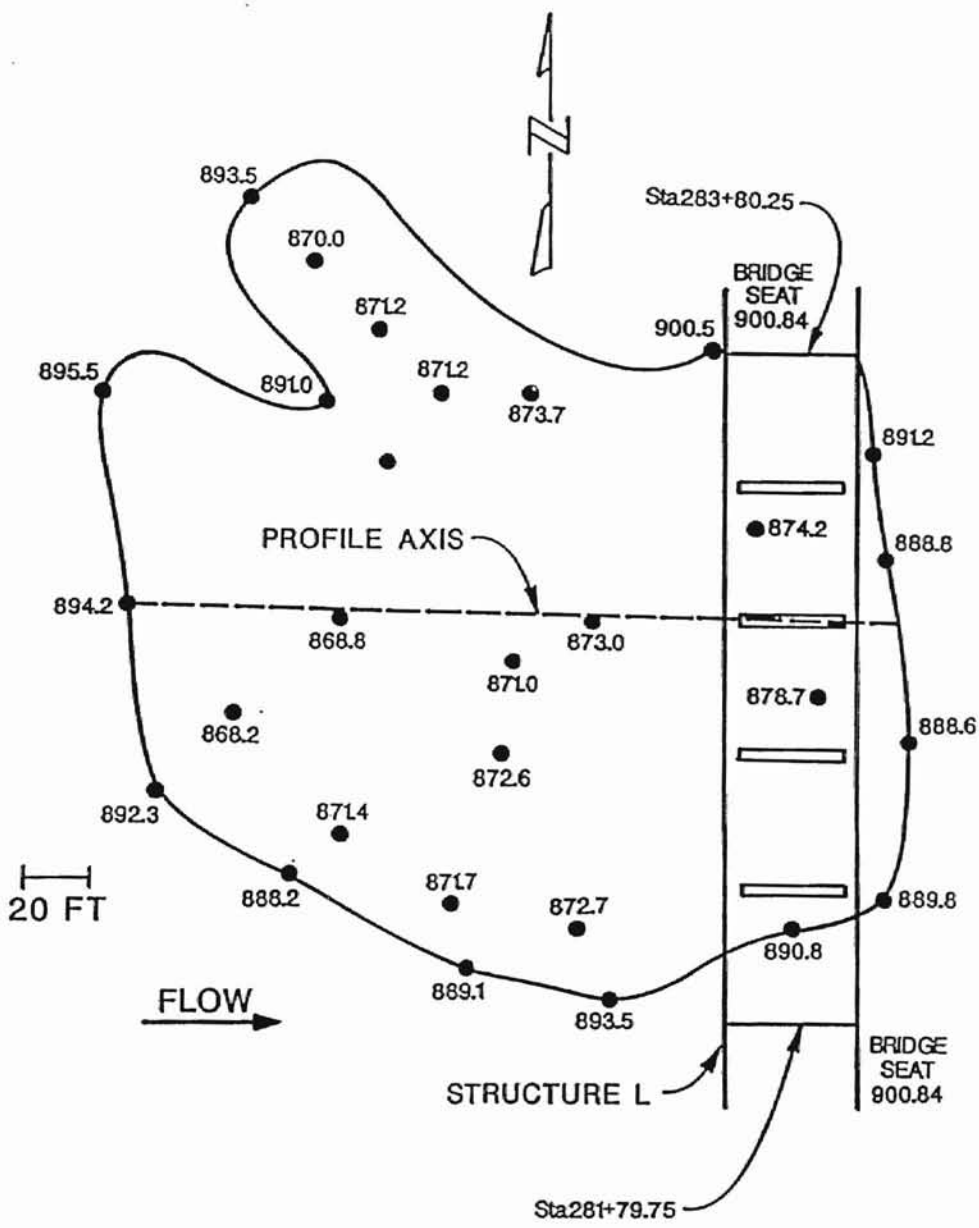

Figure 10. Location of Scour Hole Upstream of Structure L.

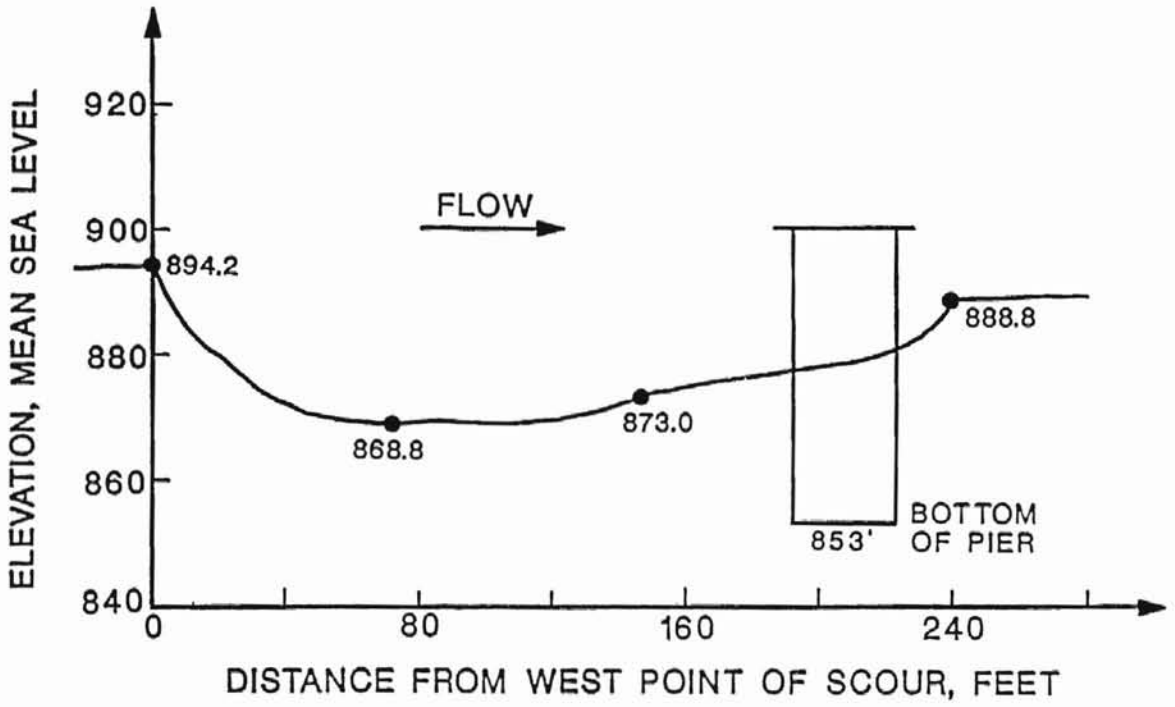

Figure 11. Profile of Scour Hole Upstream of Structure L.

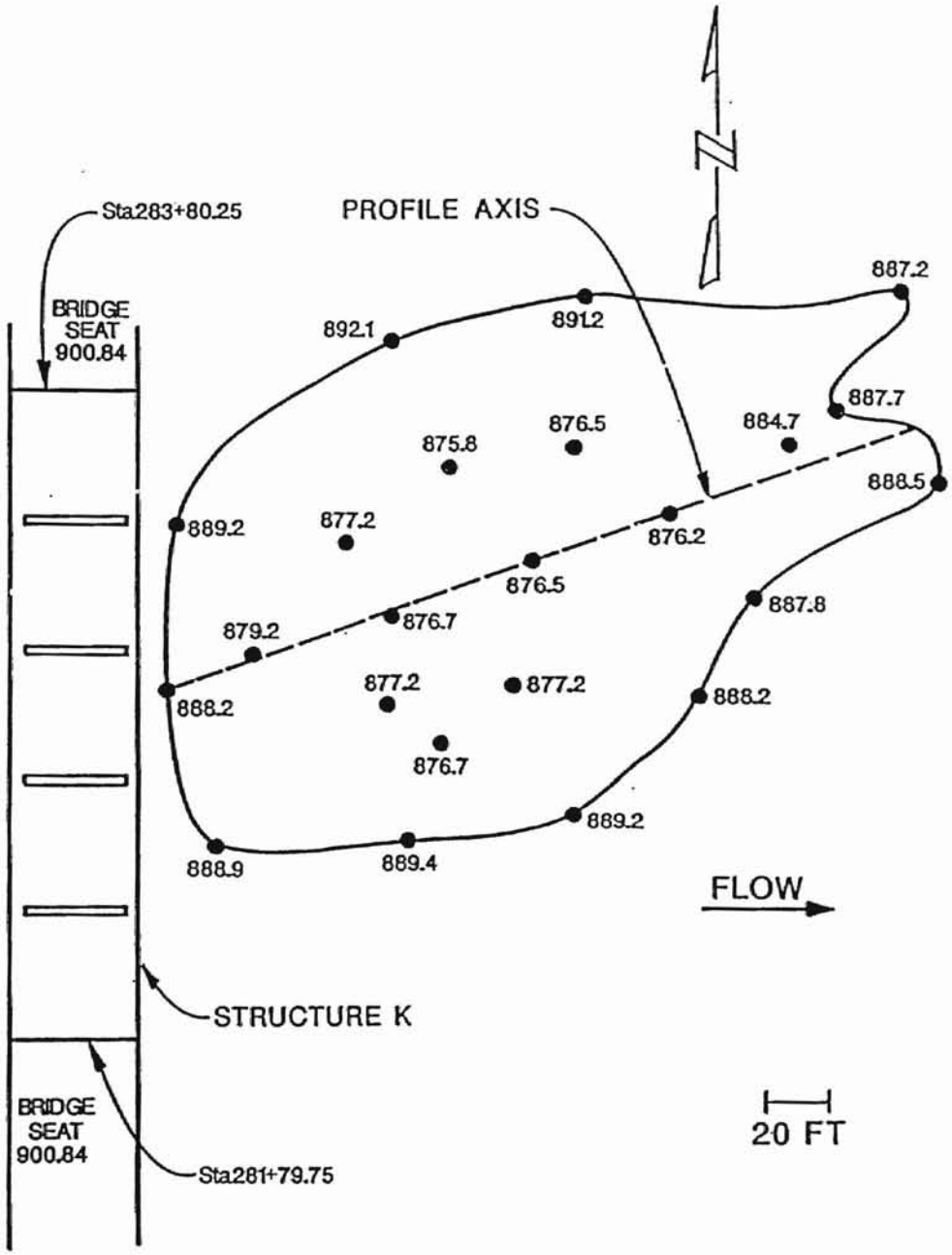

Figure 12. Location of Scour Hole Downstream of Structure K.

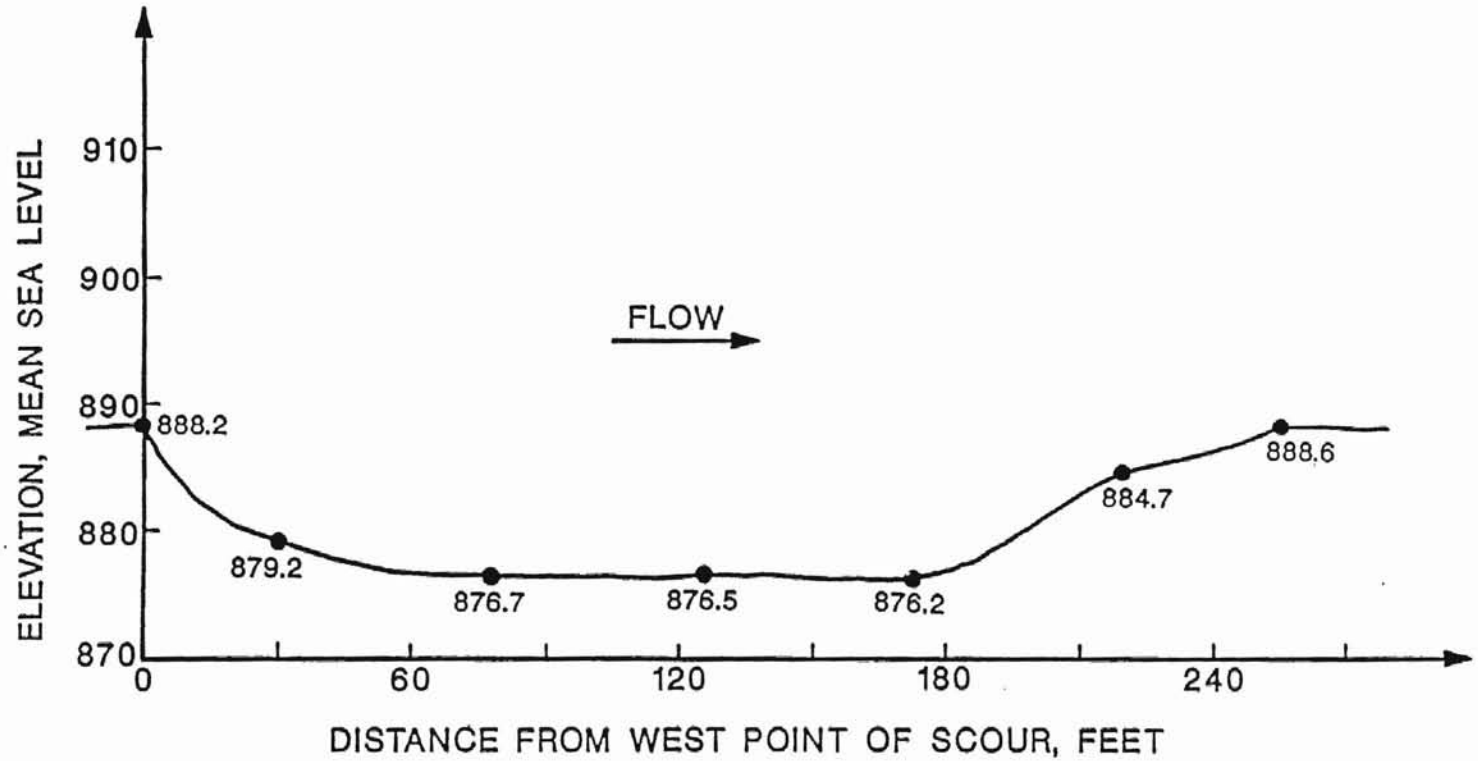

Figure 13. Profile of Scour Hole Downstream of Structure K.

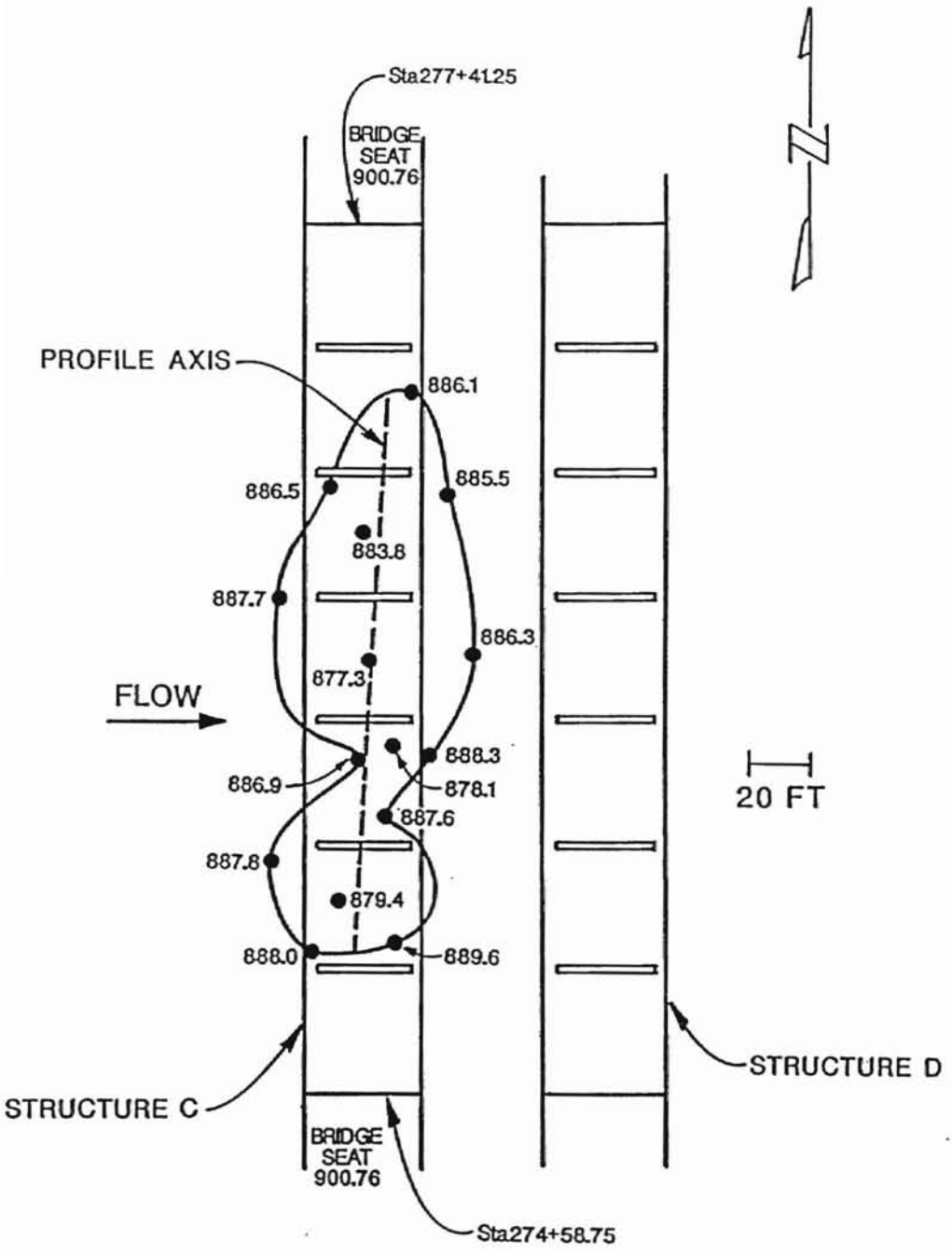

Figure 14. Location of Scour Hole Upstream of Structure C.

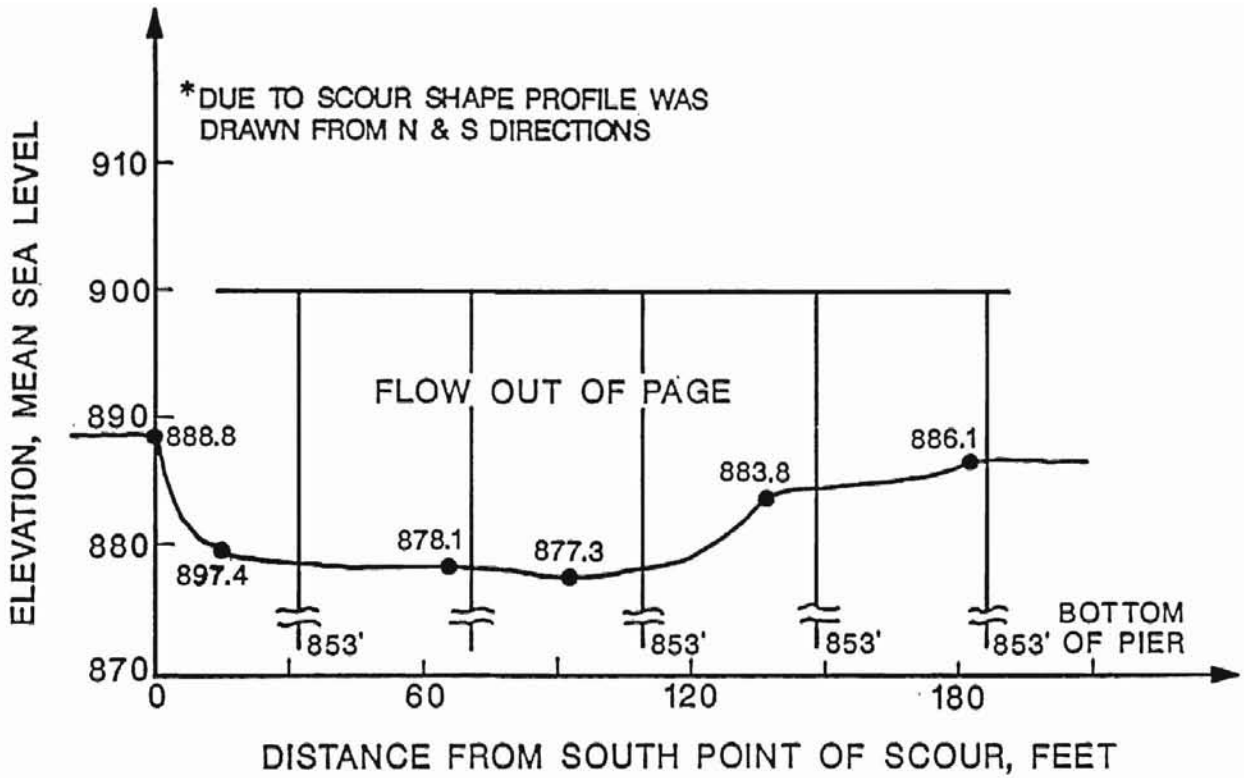

Figure 15. Profile of Scour Hole at Structure C.

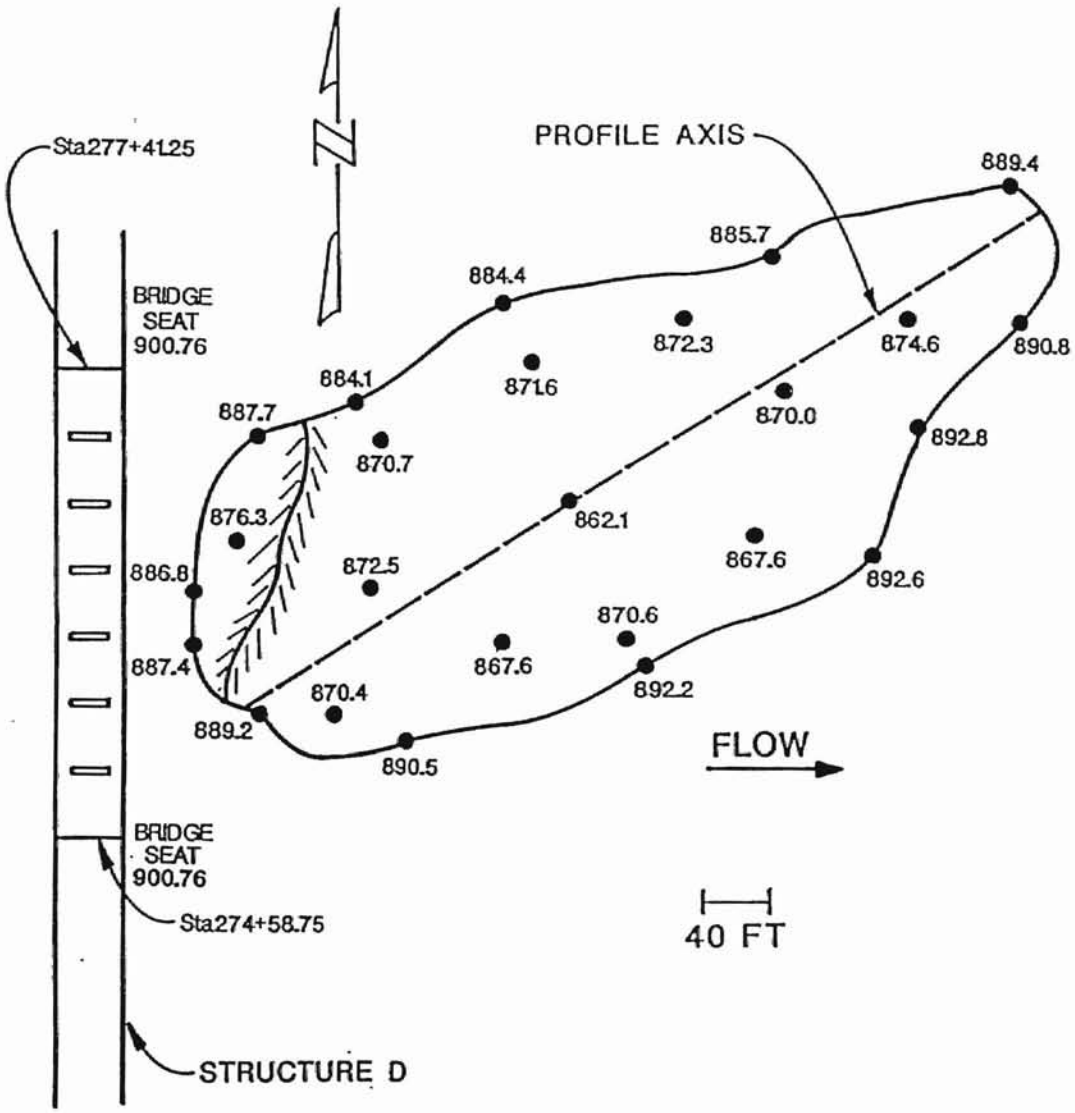

Figure 16. Location of Scour Hole Downstream of Structure D.

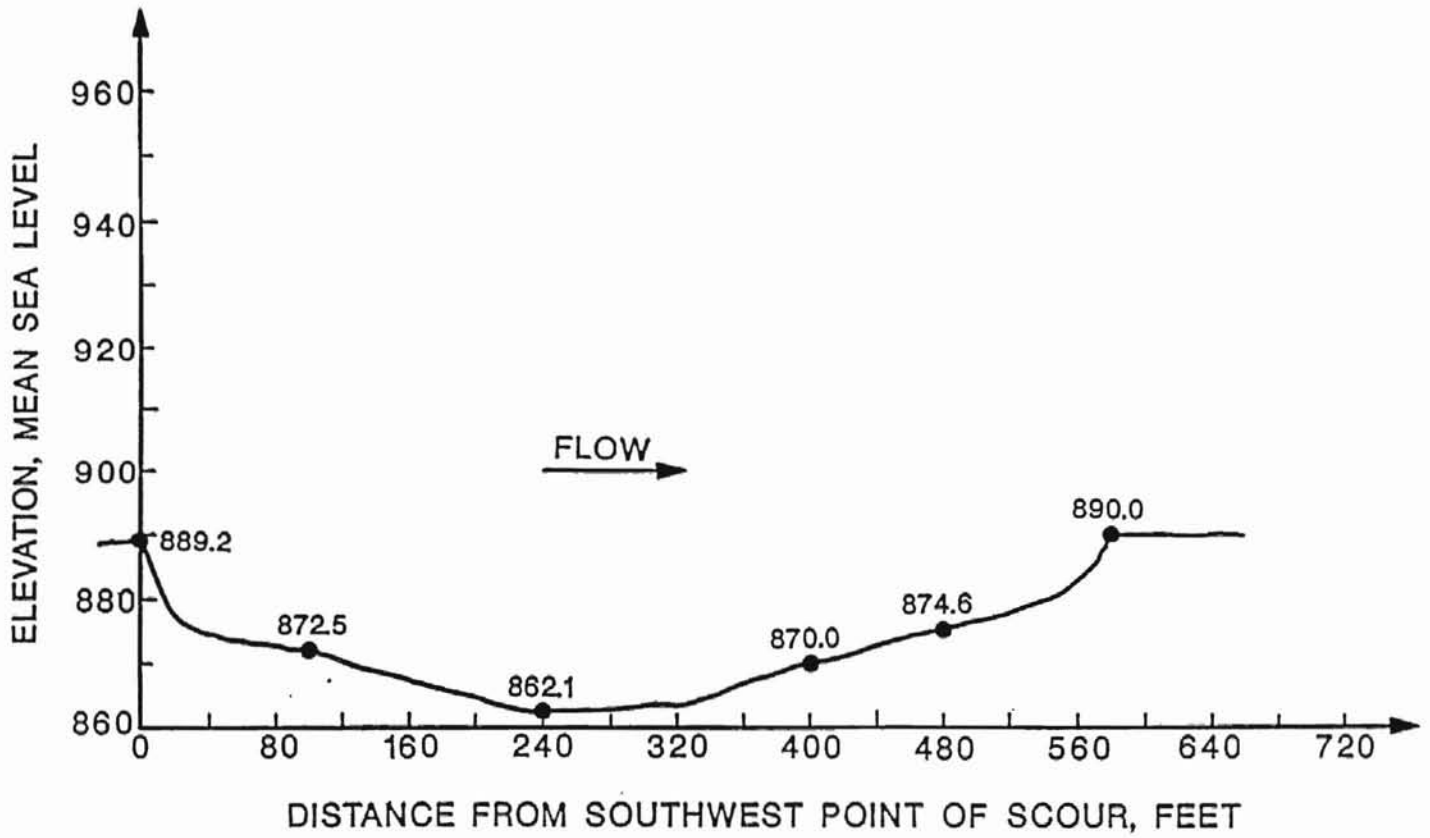

Figure 17. Profile of Scour Hole Downstream of Structure D.

APPENDIX E

CALCULATED SCOUR DATA

*** PIER SCOUR REPORT ***

Pier No.	Pier Width (ft)	Pier Lngth (ft)	Pier Nose shape	Approach Flow Vel (ft/s)	Approach Flow Depth (ft)	Approach Flow Angle (deg)	Scour Depths Local (ft)	Scour Depths Genrl (ft)	Scour Depths Total (ft)	Riprap D50 (ft)
1	1.33	6.65	Square	8.82	9.34	76.9	10.45	23.30	33.75	1.47
30	1.33	6.65	Square	6.08	11.93	83.3	9.20	17.35	26.54	.70
31	1.33	6.65	Square	4.04	12.43	86.2	7.73	.00	7.73	.31
32	1.33	6.65	Square	8.31	12.42	78.7	10.59	27.16	37.75	1.30
33	1.33	6.65	Square	6.70	12.71	86.3	9.64	20.88	30.52	.85
34	1.33	6.65	Square	7.74	12.92	77.0	10.33	25.63	35.96	1.13
35	1.33	6.65	Square	7.09	12.99	81.6	9.95	22.93	32.87	.95
36	1.33	6.65	Square	8.19	13.12	79.3	10.60	27.86	38.46	1.26
37	1.33	6.65	Square	8.61	13.09	80.0	10.83	29.63	40.47	1.40
38	1.33	6.65	Square	9.54	12.97	82.4	11.29	33.28	44.58	1.71
39	1.33	6.65	Square	8.83	13.07	79.4	10.95	30.48	41.43	1.47
40	1.33	6.65	Square	6.85	12.83	85.5	9.75	21.66	31.41	.88
41	1.33	6.65	Square	5.11	13.03	73.2	8.63	.00	8.63	.49
42	1.33	6.65	Square	6.92	12.17	65.3	9.61	21.10	30.71	.90
43	1.33	6.65	Square	5.94	12.55	85.6	9.14	17.39	26.53	.66
44	1.33	6.65	Square	9.54	12.79	73.5	11.26	32.91	44.17	1.71
45	1.33	6.65	Square	9.61	12.64	79.9	11.30	32.89	44.19	1.74
46	1.33	6.65	Square	8.49	11.62	76.4	10.59	26.49	37.08	1.36
47	1.33	6.65	Square	9.15	11.43	77.0	10.91	28.61	39.53	1.58
48	1.33	6.65	Square	8.45	8.60	84.6	10.12	20.70	30.82	1.34
49	1.33	6.65	Square	5.78	10.26	88.8	8.75	14.37	23.12	.63
50	1.33	6.65	Square	5.56	10.90	85.6	8.72	14.18	22.89	.58
51	1.33	6.65	Square	8.34	11.20	81.1	10.46	25.15	35.61	1.31
52	1.33	6.65	Square	8.14	11.18	84.8	10.32	24.37	34.69	1.25
53	1.33	6.65	Square	8.20	11.74	81.0	10.45	25.57	36.01	1.27
54	1.33	6.65	Square	8.66	11.51	81.8	10.67	26.94	37.60	1.41
55	1.33	6.65	Square	8.19	11.96	82.5	10.46	25.91	36.37	1.26
56	1.33	6.65	Square	9.14	11.44	81.5	10.91	28.62	39.53	1.57
57	1.33	6.65	Square	8.61	11.43	85.0	10.60	26.60	37.20	1.40
58	1.33	6.65	Square	8.55	11.00	79.2	10.55	25.55	36.10	1.38
59	1.33	6.65	Square	7.88	10.58	79.5	10.13	22.39	32.52	1.17
60	1.33	6.65	Square	6.74	10.70	72.3	9.45	18.42	27.87	.86
61	1.33	6.65	Square	6.25	9.80	82.1	9.07	15.51	24.58	.74
62	1.33	6.65	Square	5.59	10.63	81.3	8.74	14.04	22.78	.59
63	1.33	6.65	Square	8.83	11.37	77.4	10.74	27.29	38.03	1.47
64	1.33	6.65	Square	9.17	11.17	84.7	10.86	28.15	39.01	1.58
65	1.33	6.65	Square	8.97	11.02	81.2	10.77	27.13	37.90	1.52
66	1.33	6.65	Square	9.58	10.34	83.5	10.96	27.87	38.83	1.73

Note - Pier scour calculated using CSU equation.

VITA

Michael T. Buechter

Candidate for the Degree of

Master of Science

Thesis: SCOUR ANALYSIS OF THE INTERSTATE-35 AND CIMARRON RIVER CROSSINGS USING THE FESWMS-2DH AND SMS COMPUTER MODELS

Major Field: Civil Engineering

Biographical:

Personal Data: Born in St. Louis, Missouri, on August 20, 1966, the son of Emil and Estelle Buechter.

Education: Graduated from Kemper Military School and College, Boonville, Missouri in May 1984. Received Associates of Arts Degrees in Mathematics, Engineering Science, and General Transfer Studies from Florissant Valley Community College in December 1988. Received a Bachelor of Science Degree in Civil Engineering from the University of Missouri at Rolla, Missouri, in May 1990. Completed the requirements for the Master of Science degree with a major in Civil Engineering at Oklahoma State University in May, 1997.

Experience: Employed by the Oklahoma Department of Transportation as an Engineering Intern from 1990 to 1995. Employed by Booker Associates, Inc., an architectural and engineering firm, from 1995 to the present.

Professional Memberships: American Society of Civil Engineers.